Investigating the Design and Manufacture of PneuNet Actuators as a Prosthetic Tongue for Mimicking Human Deglutition

by

Francis Darmont Araya

A Thesis

Submitted to the Faculty

of the

WORCESTER POLYTECHNIC INSTITUTE

in partial fulfillment of the requirements for the

Degree of Master of Science

in

Mechanical Engineering

April 28, 2019

APPROVED:

Professor Pradeep Radhakrishnan, Advisor

Professor John M. Sullivan, Committee Member

Professor Robert Daniello, Committee Member

Professor Cagdas D. Onal, Graduate Committee Representative

Abstract

The number of Total Glossectomy cases in the United States is seeing an increasing trend as per the Nationwide Inpatient Sample Database. Patients, who have undergone such aggressive surgical procedures, have extensive limitations performing basic oral functions such as swallowing (deglutition), eating and speaking. Current rehabilitation prostheses do little in restoring the functionality of the original tongue. This is true especially in deglutition, which is necessary to transfer a bolus to the esophagus. Such patients need advanced prosthetic devices and through this research, investigations into potential solutions for prosthetic tongues to aid in deglutition were carried out.

The process began with an extensive literature review that provided tongue position, motion, and pressure data during the swallowing stages. Several potential designs were considered such as using linkages and pneumatic networks (PneuNets). Based on a decision matrix, PneuNets were adopted as the foundational basis for generating prosthetic designs. Several prototypes were fabricated using Fused Filament Disposition for mold development and silicone Eco-flex 00-30 for actuator development. Each iteration involved tackling several design and manufacturing challenges especially when scaling these actuators from an initial experiment to an anatomical shape and size of a human tongue. A tongue of dimensions 1.8 inches wide, 2.4 inches long and 0.24 inches thick was developed.

The PneuNet actuator was powered by a pneumatic system and kinematic data was collected using a tracking software. The data gathered provided validation comparisons between position trends exhibited in the literature. Theoretical deflection models were generated for analyzing the deflection of the front, middle and back sections of the tongue prototype. Details from literature review, design iterations, simulations, validation processes, research challenges and conclusions will be discussed in depth.

Acknowledgements

I would like to thank Professor Pradeep Radhakrishnan, Assistant Teaching Professor, Mechanical Engineering Department, WPI for his guidance and support through this thesis research. I would also like to thank the following people who were instrumental through this research process: Professor Cagdas Denizel Onal, Associate Professor, Mechanical Engineering Department, for his silicone actuator design ideas; Professor John M. Sullivan, Associate Department Head, Mechanical Engineering Department, for his mechanical design approach ideas; Professor Robert Daniello, Assistant Teaching Professor, Mechanical Engineering Department; for his validation and testing recommendations; Peter Hefti, Lab Manager, ME Experimentation Laboratory, for his assistance with Arduino controls accessories; Barbara Edilberti, Administrative Assistant, Graduate Department, for her support with thesis committee formulation; Barbara Furhman, Administrative Assistant, Undergraduate Department, for her support with ordering project items; Logan Chen, Undergraduate Student, Mechanical Engineering Department, for his support in research design; Rebecca Mendivil, Graduate Student, Robotics Engineering Department, for the simulation ideas; Morris Chung, Graduate Student, Robotics Engineering, for PneuNet idea preliminary experimentation; Augusto Duran, Graduate Student, Mechanical Engineering Department, for PneuNet scholarly research; Ron Holiman, Doctor of Dental Science, for his dental equipment support; Shaina Darmont, Doctor of Dental Science, for her continued support and guidance in this research.

Glossary

Apex: the uppermost point

Bolus: a rounded mass

Cast: to give a shape to (a substance) by pouring in liquid or plastic form into a mold and letting harden without pressure

Chimerize: to turn into

Deglutition: the act or process of swallowing

Denture: an artificial replacement for one or more teeth

Dorsal: an ornamental cloth hung behind and above an altar

Endosseous: of or pertaining to any object placed or contained within a bone

HTV and RTV: Silicone Materials

Laryngopharynx: the lower part of the pharynx lying behind or adjacent to the larynx

Magnetic: of or relating to a magnet or to magnetism

Mandibular: a lower jaw consisting of a single bone or of completely fused bones

Mastication: to grind or crush (food) with or as if with the teeth

Maxillary: an upper jaw especially of humans and other mammals in which the bony elements are closely fused

Mucocutaneous: made up of or involving both typical skin and mucous membrane

Nasopharynx: the upper part of the pharynx continuous with the nasal passages

Obturator: something (such as a prosthetic device) that closes or blocks up an opening (such as a fissure in the palate)

Oropharynx: the part of the pharynx that is below the soft palate and above the epiglottis and is continuous with the mouth

Phonation: to produce vocal sounds and especially speech

PneuNet: Pneumatic Networks

Proprioceptive: of, relating to, or being stimuli arising within the organism

STL: Standard Triangle Language

Table of Contents

Table of Figures

Table of Tables

I. Introduction

The study of the human body has undoubtedly increased our understanding of human motion. Specifically, the ability to quantify and simulate this motion, has enabled advancements in the field of medicine, rehabilitation and psychology furthering the effectiveness of each discipline. With advancements in technology, the interdisciplinary approach of the mechatronics field has enabled greater control of mechanisms mimicking human motion. A prime example of this can be seen in Figure 1 (reproduced as is from [1]) , of a neurally controlled modular robotic arm whose design was completed in 2009 by the University of John Hopkins Applied Physics Laboratory [1]. Composed of 22 plus degrees of freedom and up to 21 electric motors, the bionic arm neurally controlled ability has revolutionized the prosthetic industry and increased the quality of life of Johnny Matheny, an arm cancer patient currently wearing the device [2].

Figure 1 Neurally controlled robotic arm demonstrating gripping capabilities (reproduced as is from [1]).

Another example of these advancements can be seen in what is known as the "Organ Care System" in Figure 2 (reproduced as is from [3]). Developed by Transmedic Inc., the organ transplant care system, currently in US clinical trials, is on track to revolutionize the standard care of transplant organs. Composed of a gas-powered pump and electronic system, the module revives and maintains the health of organs as the heart by supplying it with the nutrients and environment while in route to the patient in need [4]. Although there are many more trials to take place, this system could potentially reduce the chances of a heart degradation that occurs through the standard ice and cooler transportation method.

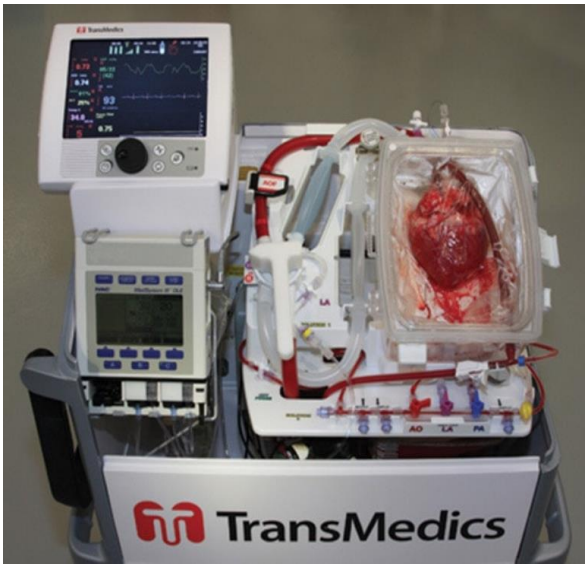

Figure 2 Organ Care System for supporting a heart transplant (reproduced as is from [3]).

Major factors in the advancement of technologies previously mentioned, are directly related to their physical location and scale. The accessibility of these body parts allows for the use of advanced motion analysis technology currently available. This attribute, aids in allowing vast amount of data to be collected, increasing the understating of the body parts function and anatomy. Furthermore, its scalability, in comparison to other smaller organs, increases the implementation feasibility of supporting and advanced design mechanisms.

Unfortunately, this vast amount of data is not always for all organs, and associated disciplines. In particular, the discipline of oncology rehabilitation, has been identified by this research as a field in which such lack of data has reduced the advancements of tongue prosthetic devices. The use of tongue prostheses is primarily associated with patients who have undergone what is known as a Total Glossectomy. This surgical procedure resects the tongue from the oral cavity, as a means of mitigating the spread of oral cancer cells. This is an aggressive surgical procedure, that results in a long rehabilitation process to regain the ability to swallow, eat and speak. The lack of experimental data on the function of the tongue and awareness of this debilitating condition, has reduced the advancements of prosthetic technology, leaving post-Glossectomy patients with little oral functionality.

In the following chapters, supporting background information on statistics, total glossectomy procedures, current prosthetic devices and tongue swallowing stages are provided. An extensive literature review on kinematic and pressure data of the tongue, and current tongue

mechanical designs in industry was performed. Mechanical designs in industry are analyzed for their usefulness in fulfilling the swallowing motion. Finally, the prototype design, manufacture, testing and validation is provided in detail.

II. Oral Cancer and Rehabilitation Methods

This chapter provides statistical data supporting the importance of cancer and the increase of total glossectomy cases in the United States. Current rehabilitation efforts including surgical and prosthetic approaches are presented and analyzed for their effectiveness in restoring oral function. Tongue anatomy and swallowing stages are presented the describe the complexity of the task.

Oral Cancer Statistics

The statistical analysis performed by the National Cancer Institute considers cancer to be not only a major public health in the world but also the second leading cause of death in the United States as projected for 2018 [5]. Accounting for 3% of all new cases in the U.S., oral cavity and pharynx cancers are among the top 10 leading cancer types. It is estimated for the year 2018 that 51,540 new cases of oral cancer will be recorded [6]. This reflects the recorded 0.7% increase per year of new cases in the last 10 years [6]. Specifically, data from the Nationwide Inpatient Sample, composed of 133,850 patients, has noted an increase in Total Glossectomy surgical cases as shown in Figure 3 ranging from 1993-2000 to 2001-2010 [7].

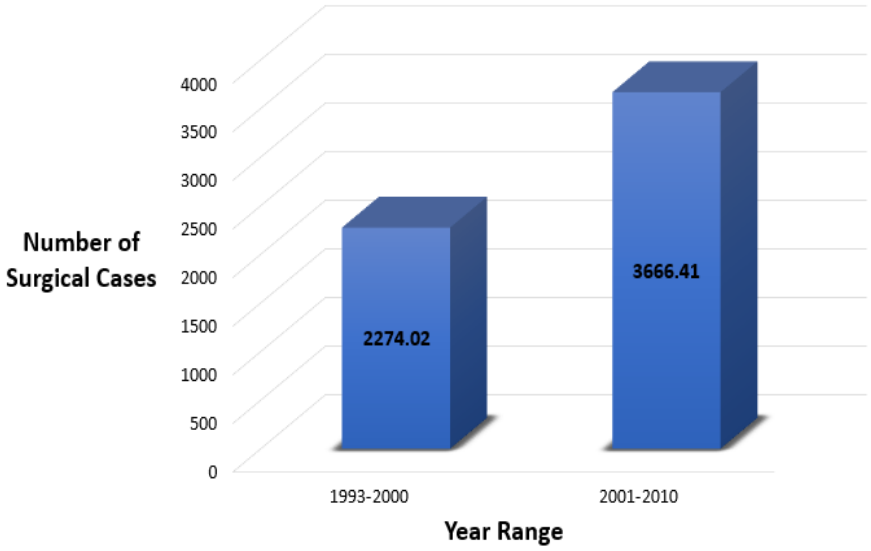

Figure 3 Nationwide Inpatient Sample Data of the number Total Glossectomy surgical cases [7].

Although a single probable cause cannot be determined due to the varying factors involved, some common causes have been identified as relating to tobacco and alcohol use. In addition, a less known common cause is the sexually transmitted disease Human Papillomavirus (HPV).

Current Rehabilitation Efforts

Current post-glossectomy rehabilitation interventions entail several treatments options in hopes of speeding rehabilitation efforts and increasing quality of life. These treatments include surgical and prosthetic approaches.

Surgical Approach

The surgical approach for rehabilitation seeks to reconstruct the floor of the mouth with human flesh to facilitate the retention of foods and liquids for total glossectomy patients. Several techniques are used in this approach and they include the double tongue method, manta ray flap technique and the mushroom-shaped flap.

The double tongue technique shown in Figure 4 (reproduced as is from [8]), uses the rectus abdominis muscle and creates a double layered flap that fills the floor cavity of the mouth. This method is recommended for patients whom the larynx is preserved.

Figure 4 Double Tongue surgical technique (reproduced as is from [8]).

The manta ray flap technique shown in Figure 5 (reproduced as is from [9]) uses the patients donor site flesh at the appropriate pedicle orientation for exact fit reconstruction. Some of the advantages of this procedure include long pedicle length, minimal donor site morbidity and the ability to chimerize with available muscle [9].

Figure 5 Manta Ray Flap surgical technique (reproduced as is from [9]).

Mushroom-shaped Flap technique shown in Figure 6 (reproduced as is from [10]), usually performed on sub-total glossectomy patients, uses the anterolateral thigh perforator flap to reconstruct the tongue anatomy. This procedure was found to be innovative and effective option for subtotal tongue reconstruction.

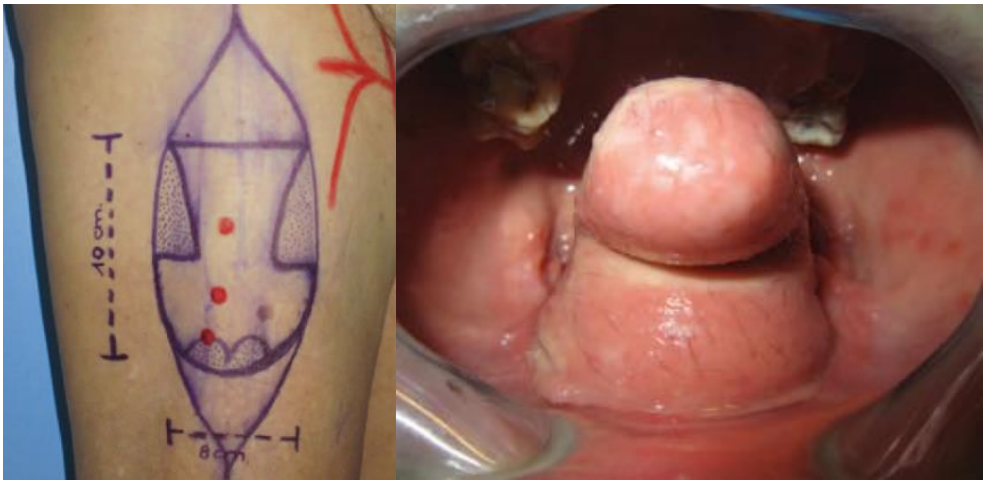

Figure 6 Mushroom-shaped Flap surgical technique (reproduced as is from [10]).

Although advancements of each technique continue to evolve, the results of such procedures have yet to be individually satisfactory. A journal review, presented by Carvalho et al. [11], found that common problems with a free flap surgical approach includes its low effectiveness in providing the intended movement, pressure to transport bolus and its restrictiveness to the pharyngeal opening [11].

Prosthetic Approach

The prosthetic approach entails the use of oral prosthetics. This approach is generally taken to mitigate surgical prognosis that find the affected area to be poor and too large for reconstructive surgery. In addition, it allows for rapid results with minimal pain to the patient. The general composition of such a prosthetic is determined and classified by its attachment structure. These prosthetics include the maxillary obturator, mandibular denture, magnetic cast and implant retained.

The maxillary obturator (reproduced as is from [12]) shown in Figure 7 is generally used on patients with maxillofacial defects as (reproduced as is from [12]) shown in Figure 8 and its supported by the remaining teeth and palate using Adam's and C clasps. The structure of the prosthetic is composed of acrylic and incorporated stainless steel. Generally, its use provides restored mastication, swallowing, resonance and speech. Although the effectiveness of this prosthetic is dependent on the severity of the defect and the recovery of surrounding tissues, it is generally successful in restoring mouth motion with additional rehabilitation [12].

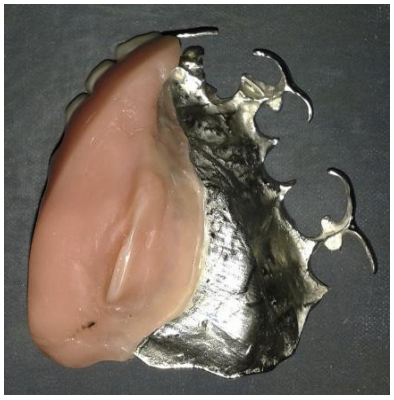

Figure 7 Hard palate prosthetic encompassing Adam and C clasps (reproduced as is from [12]).

Figure 8 Hard palate post-surgery defect (reproduced as is from [12]).

Another oral prosthetic type is known as the magnetic cast prosthesis. The assembly is composed of a polish cobalt RPD framework (Figure 9 reproduced as is from [13]) and acrylic resin base (Figure 10 reproduced as is from [13]). Cobalt-samarium magnets are incorporated in the acrylic resin base to facilitate the attachment of the tongue component. The tongue component is made of silicone material and primarily assists the patient with speech. Some of the disadvantages include the magnet corrosion, wear and loss. Generally, the prosthetic provides swallowing and speech improvement. Pathologist evaluation is generally recommended in conjunction with the implementation of this prosthetic [13].

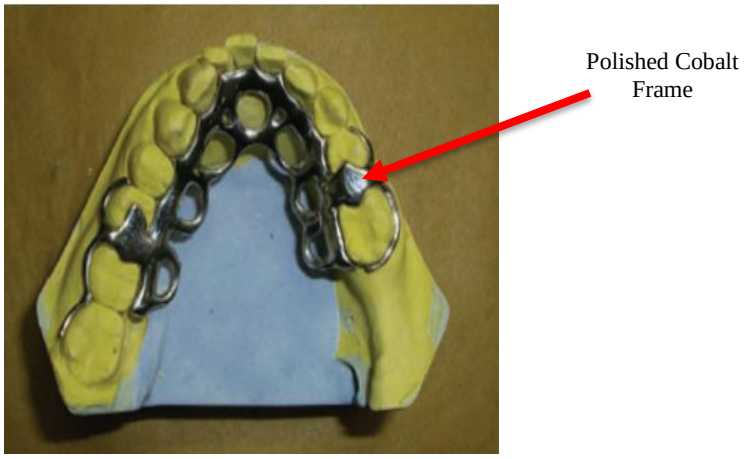

Figure 9 Magnetic cast prosthesis polish cobalt RPD framework (reproduced as is from [13]).

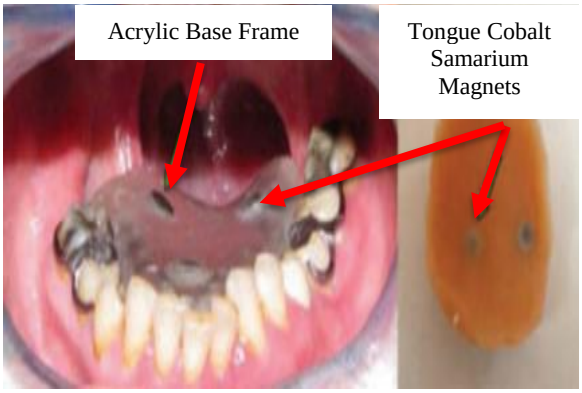

Figure 10 Magnetic cast prosthesis depicting location of the embedded magnets (reproduced as is from [13]).

Another oral prosthetic type is known as the implant supported prosthetic. This prosthetic utilizes five endosseous implants 3.74 mm in diameter and 13 mm in length that are secured to the patient's jaw bone. Semi-anatomic acrylic resin artificial teeth are created along with lingual funnel

shaped contours (Figure 11 reproduced as is from [14]) on the prosthetic upper surface to direct food into the esophagus. A noble gold alloy structure shown in Figure 12 and Figure 13 (reproduced as is from [14] is used as the supporting structure for the implant attaching surface. The prosthetic was designed to be detachable and without a tongue due to the severity of the defect and to ensure oral hygiene. The patient that used this prosthetic was able to begin eating semi-solid foods after two years of use [14]. Due to the lack of tongue structure, this prosthetic was not able to improve the speech of the patient.

Figure 11 Implant supported prosthetic top view (reproduced as is from [14]).

Figure 12 Implant supported prosthetic bottom view (reproduced as is from [14]).

Figure 13 Implant supported prosthesis mounting frame work (reproduced as is from [14]).

Finally, full denture prostheses are used for total reconstruction of the teeth and tongue edentulous patients. The denture shown in Figure 14 (reproduced as is from [15]) was designed for a patient that underwent total glossectomy and a mucocutaneous flap reconstruction. The prosthesis is composed of a silicone (molloplast-B) tongue and acrylic base and teeth. The silicone tongue is designed to be arched at the anterior one third and at a 15-degree angle on the tip. The prosthesis works as a denture in which it is held in place by the suction created between the denture and the floor of the mouth with the aid of saliva. Several trials and adjustments are performed with the patient and speech therapist to obtain the best fit and effectiveness possible. Noticeable comfort and oral functional improvements are noticeable after six months of use. The finished look of an installed full denture prosthetic in Figure 15 (reproduced as is from [15]).

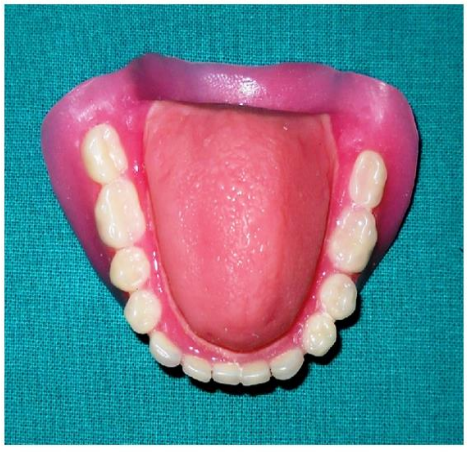

Figure 14 Silicon (molloplast-B) and acrylic based denture prosthesis (reproduced as is from [15]).

Figure 15 Front view of patient with full denture tongue prosthesis (reproduced as is from [15]).

Although the prosthesis previously mentioned provide esthetic and static functionality of the tongue, little improvement has been accomplished to recreate the kinematic function of the original muscular organ. In turn, patients must undergo months of readjustments and speech therapy to adapt and reprogram their oral movements. Furthermore, adapting to these intervention methods are only the underlying difficulties associated with the resection of the tongue. Psychological effects as depression have also been identified to have an increased correlation with head and neck cancer patients in response to visible changes in their oral physique motion due to swallowing difficulties or feeding tube requirements. Although the severity of symptoms varies due to major factors as patients social support, it has been found that associated depression symptoms can last up six years post treatment [16]. Although both surgical and prosthetic approaches provide beneficial characteristics for rehabilitating patients, their advancements have yet to reach levels of noticeable improvements. The following chapter provides in detail the research focus and methodology used to investigate the design and manufacture of tongue prosthesis.

III. Research Statement and Methodology

This chapter describes the research statement and methodology of this research. Information on the focus of each chapter is provided in detail.

Research Statement

Based on the background information related to oral cancers and their rehabilitation, this research seeks to do the following:

Investigate various design and manufacturing aspects related to a prosthetic tongue by

- *identifying available tongue motion data*
- *researching existing mechanical designs and identifying suitable foundational designs*
- *investigating the manufacturing processes, development challenges and existing theoretical deflection models to compare prototype experimental data*

Considering the complexity of the tongue muscle and its limiting location, this research seeks to only understand, quantify and mimic the deglutition function of the human tongue. The next section describes the methodology adopted to fulfil the various aspects of this research.

Methodology

The method taken to develop a prosthetic tongue began by carrying out an extensive literature review, performing an actuation selection process, investigating the design and manufacture of PneuNets actuators, developing prototype testing controls and performing validation processes.

Chapter IV, Literature Review, provides information that explains the tongue's function and anatomy, current tongue mechanisms, and industry significance. The information gathered in this chapter supports the investigative research process by identifying the important functional parameters to consider when developing the swallowing motion.

Chapter V, Actuation Selection, provides information that explains the process taken to determine and select the appropriate mechanism for use as a foundational design, the governing equations of the foundational design and the application of such mechanism in industry. The information provided in this chapter, supports the use of PneuNets as a means of developing a

prosthetic tongue. Furthermore, it provides quantitative measure for making the necessary changes to future design iterations.

Chapter VI, Design and Manufacture of PneuNets Actuators, investigates the foundational design mechanism structure by attempting to recreate it using Fused Filament Fabrication (FFF). Based on this trial iteration, tongue shaped silicone actuator iterations are developed, and information related to the manufacturing process, challenges and learned outcomes are provided. The information provided in this chapter, seeks to increase the available data regarding the fabrication of PneuNet actuators and identify critical details to ensure success and repeatability of the manufacturing process.

Chapter VII, Controls for Prototype Testing, provides information that explains the process taken to develop a testing module for the prototype. This chapter seeks to provide information related to the necessary controls for actuating such PneuNet systems.

Chapter VIII, Validation and Discussion, provides information that explains the process taken to track the position, speed and acceleration of the different sections of the tongue prototype. Analysis of contributing factors to the inconsistency of the data is provided.

Chapter IX, Conclusions and Future Work, provides information related to the challenges, ongoing work and future work. Conclusions about the work performed in this research are presented in detail.

IV. Literature Review

This chapter provides a detail review of the research literature related to the function and anatomy of the tongue, kinematic and pressure data, and tongue mechanisms in industry. Fundamental aspects of the tongues swallowing motion are analyzed in this section that must be considered as key functional requirements of the tongue prosthetic. Furthermore, current tongue design mechanisms are analyzed to determine the appropriate foundational design of the tongue prosthetic.

Function and Anatomy of the Tongue

The complexity of the tongue is best described by the decomposition of the anatomical structure. As shown in Figure 16 and Figure 17 (reproduced as is from [17, 18]), the tongue muscles are composed of intrinsic and extrinsic muscles. Intrinsic muscles are located within the tongue and are described as longitudinal vertical and transverse muscles. In general, intrinsic muscles allow for the change in tongue shape when masticating (chewing), deglutition (swallowing) and phonation (speaking). In contrast, the extrinsic muscles are located outside of the tongue and include the genioglossus, hyoglossus, styloglossus, and palatoglossus muscles. The genioglossus muscle provides tongue protrusion. The hyoglossus and styloglossus muscles are intermingled and provide retraction of the tongue. Finally, the chondroglossus muscle provides tongue depression in the mouth.

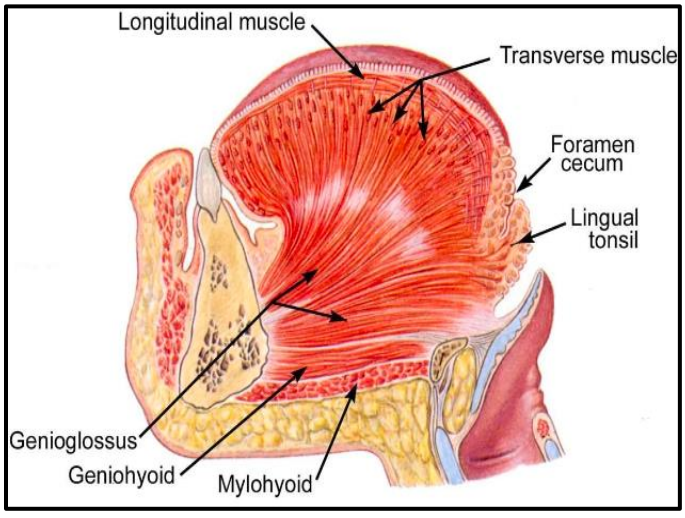

Figure 16 Intrinsic muscles of the tongue (reproduced as is from [17]).

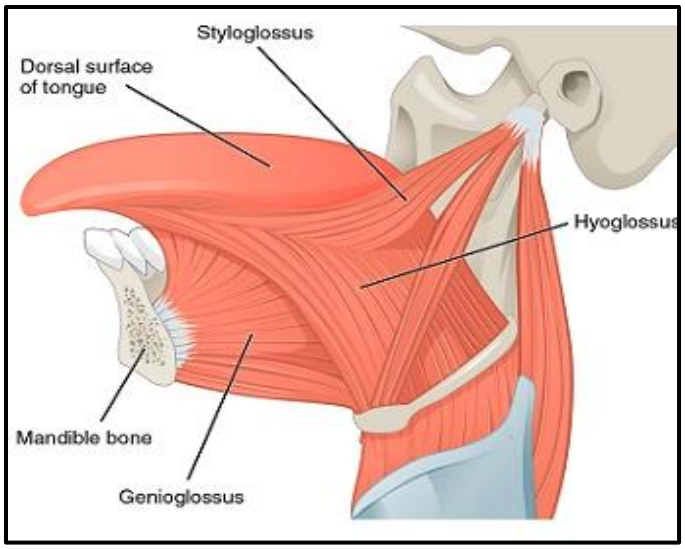

Figure 17 Extrinsic muscles of the tongue (reproduced as is from [18]).

To further understand the complexity of the tongue, it is essential to analyze its functional aspects specifically in the motion of deglutition. The deglutition process can be described in three phases which include Voluntary, Involuntary and Final Stage. Swallowing, also referred to as Deglutition, begins in the Voluntary stage when the human begins the masticate. Once a bolus, is created inside the mouth, the combination off intrinsic and extrinsic tongue muscles push the bolus to the hard palate and towards the soft palate of the mouth as shown in Figure 18 (reproduced as is from [19]).

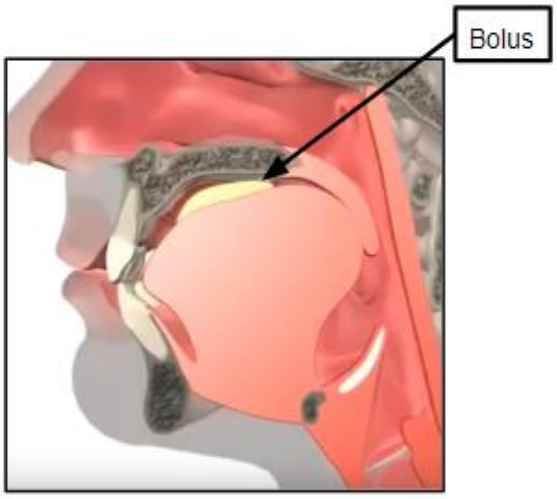

Figure 18 Voluntary deglutition process anatomy (reproduced as is from [19]).

At this point, the involuntary stage begins as the soft palate pushes the bolus to the oropharynx area while closing the nasopharynx area in the process as shown in Figure 19 (reproduced as is from [19]). This allows the bolus to continue to the laryngopharynx area without entering the nasal cavity.

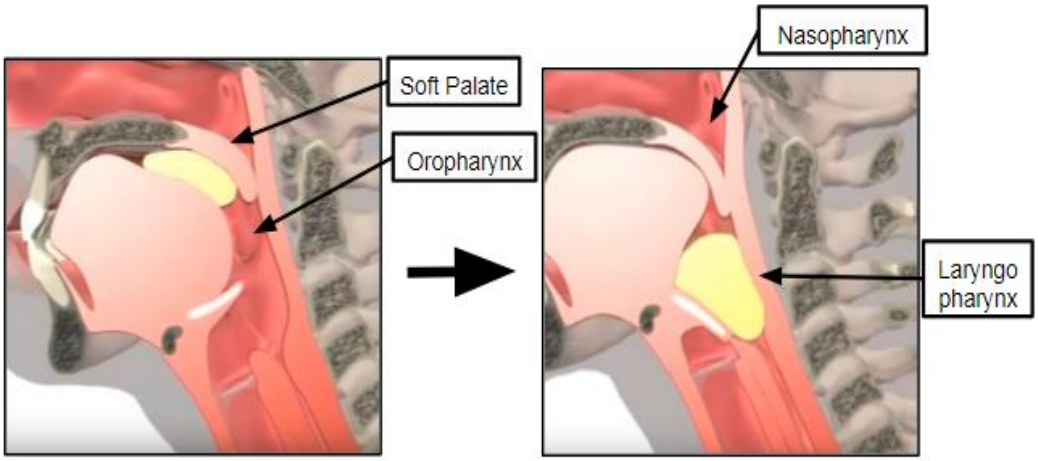

Figure 19 Involuntary deglutition process anatomy (reproduced as is from [19]).

At the final stage of deglutition, the laryngopharynx leads to the esophagus passage in which waves of muscle contractions known as peristalsis, slowly transfer the food into the stomach cavity as shown in Figure 20 (reproduced as is from [19]).

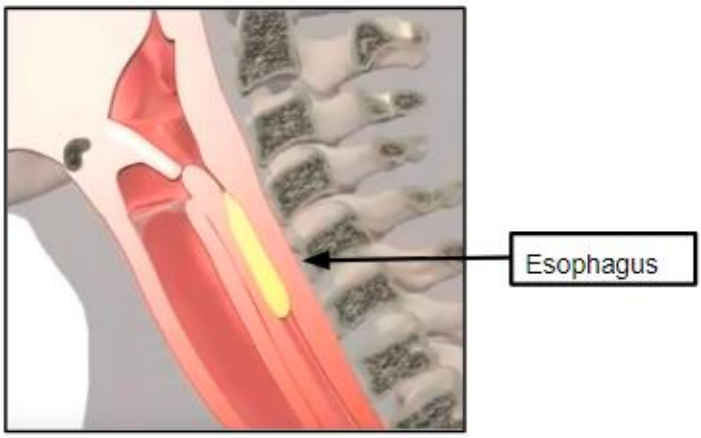

Figure 20 Final stage deglutition process anatomy (reproduced as is from [19]).

Understanding the role of the tongue in the human body, puts into perspective the overall disadvantages that Total Glossectomy patients encounter. Understanding the anatomical and functional aspects of deglutition, allow for prosthetic design considerations to be identified. For example, depending on the severity of the glossectomy, certain muscle may remain in the oral

cavity that could facilitate the movement of the mechanism. Reducing the required complexity of the system. Furthermore, it is apparent that a key element of the swallowing stages is to push the bolus to the palate. This seems to be vital in facilitating the transfer of bolus to the other areas of the tongue and into the esophagus.

Kinematic Data

A clinical test performed by the University of Wisconsin and analyzed by Tasko et al. [20], gathered tongue and jaw kinematic data of 12 healthy subjects. With the use of X-ray microbeam technology and six 2-3 mm diameter gold pellets, subjects' tongue and jaw movements were recorded as they swallowed a water bolus (mass) of 2 mL to 10 mL volume. The pellets on the tongue were positioned on the longitudinal sulcus (groove) of the tongue as shown and represented as black dots in Figure 21 (reproduced as is from [20]). The coordinate system for this experiment used maxillary occlusal plane (MaxOP) as the x-axis as and the intersection of the central maxillary incisor (MI) with the x axis plane as the y axis [20]. As an example of subject's pellet position from dorsal to apex, T1 was located at 8mm, T2 was located at 28 mm, T3 was located at 46 mm and T4 was located at 62 mm.

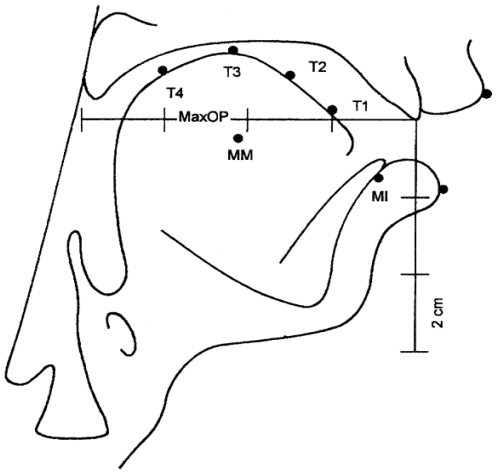

Figure 21 Gold Pellets position on the tongue and jaw (reproduced as is from [20]).

The speed of the swallowing motion was analyzed based on the T4 pellet. This was done by the study after comparison between the other tongue pellets found T4 to be the most prominent. As shown in Figure 22 (reproduced as is from [20]), T4 is represented as a central point of five swallowing replicates in a swallowing time of 1000 milliseconds (ms). This duration was chosen by the study because it included "all of the prominent tongue and jaw kinematic events" [20]. The

black circular dot represents onset point, and the white circular dot represents the peak speed position of T4 pellet. The darker lines are a representation of the average speed of the replicates [20]. The measured T4 peak speed during the swallowing motion was recorded at approximately 153 to 180 mm/s, which varied by subject's gender and the volume of water swallowed.

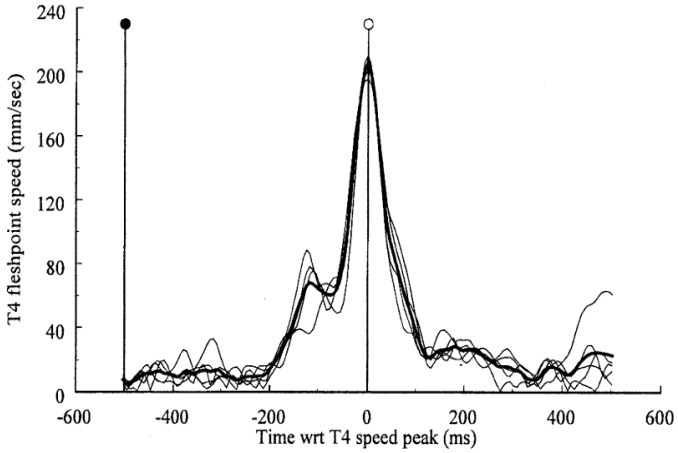

Figure 22 T4 Pellet speed from beginning to peak position of tongue swallowing motion (reproduced as is from [20]).

Using the swallowing time of 1000 ms, the positions of each pellet were also recorded and represented on Figure 23 (reproduced as is from [20]). The circular black dots represent the starting spatial position of the pellet and the circular white dots represent the positions of each pellet at their peak speed. The dark line above T3, T2 and T1 represents the Hard Palate Sagittal Outline [20].

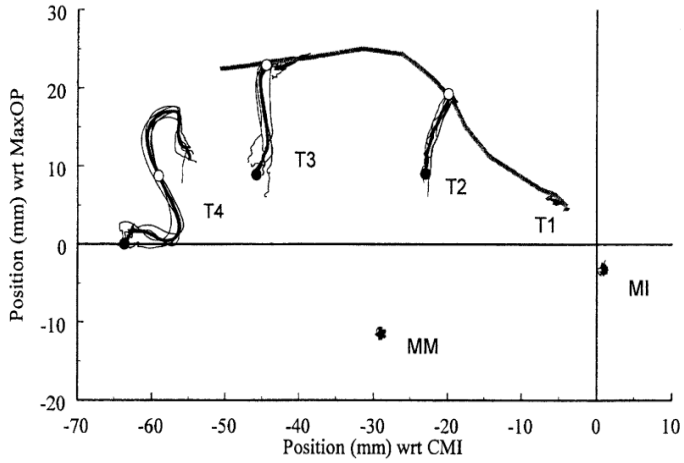

Figure 23 Pellet positions from beginning to peak speed of tongue motion (reproduced as is from [20]).

In summary, the data gathered through this clinical study is provided in Figure 24 (reproduced as is from [20]). Due to the variability of T1's results, the study did not record this point from subjects. They attribute this variability to either the immobility of the tip or the differences in bolus transfer technique by some subjects. Due to the inability of the X-Ray microbeam system to detect bolus movement, these conclusions were stated speculatively.

Based on this information, the tongue prototype design of this research will only use the data points provided. Specifically, the data points chosen for validation are for a male gender and a water swallowing volume of 10 mL. These points include T4 position of 19.1 mm, T3 position of 15.2 mm and T2 position at 10.5mm.

			Duration (ms)		Distance (mm)		Peak speed (mm/s)	
Fleshpoint	Gender		2 mL	10 mL	2 mL	10 mL	2 mL	10 mL
	M	$\bar{x}$	169	192	15.0	19.1	173	206
T4		s_y	22.5	49.2	3.54	2.38	26.0	24.0
	F	$\bar{x}$	146	151	12.0	14.1	153	180
		s_y	16.8	22.3	2.58	3.05	37.5	26.1
	M	$\bar{x}$	167	179	9.6	15.2	115	164
T3		s_y	28.8	36.1	0.53	2.92	27.8	17.4
	F	$\bar{x}$	131	152	6.1	10.0	85	129
		s_y	33.2	34.2	3.45	2.86	35.4	28.7
	M	$\bar{x}$	137	193	5.3	10.5	63	106
T2		s_y	28.1	57.60	2.38	4.53	29.4	31.0
	F	$\bar{x}$	147	139	4.7	6.4	53	78
		s_y	13.0	29.0	1.78	3.00	20.8	33.6

Figure 24 Data gathered from X-Ray Microbeam Technology (reproduced as is from [20]).

Pressure Data

Another study of importance is found in the work of Takahiro et al. [21], in which tongue pressure data was gathered on 10 healthy subjects during the swallowing motion of 15 mL volume of water. The data was recorded through the use of a palate plate that incorporated seven sensors as shown in Figure 25 (reproduced as is from [21]). The palate plate was fabricated through an impression process of each subject and constructed with pour type resin. The seven disks like pressure sensors PS2-KA were position on the palate plate based on specific anatomical landmarks [21].

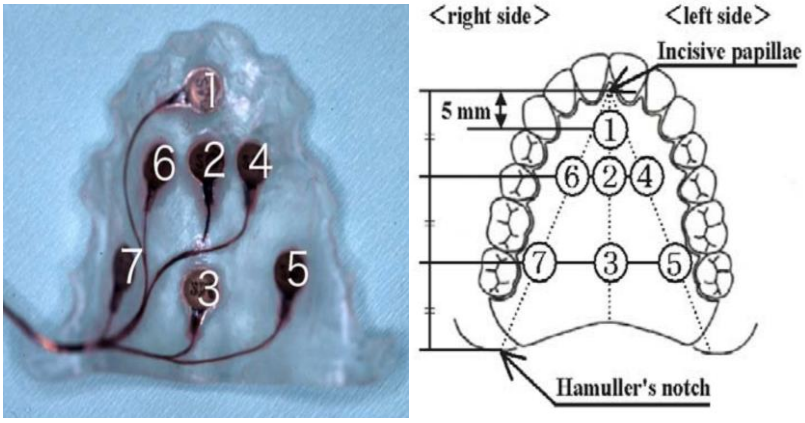

Figure 25 Palate plate with seven sensors and their anatomical positions (reproduced as is from [21]).

A graph of the data retrieved by the study is shown in Figure 26 (reproduced as is from [21]) The data from all seven sensors highlights respective Maximum Magnitude of Tongue Pressures (MP), Time of the Peak of Tongue Pressures (TPP), Time of Tongue Pressure Generation (TPG), Time of Tongue Pressure Ceasing (TPC) and Duration of Tongue Pressure (DP) [21].

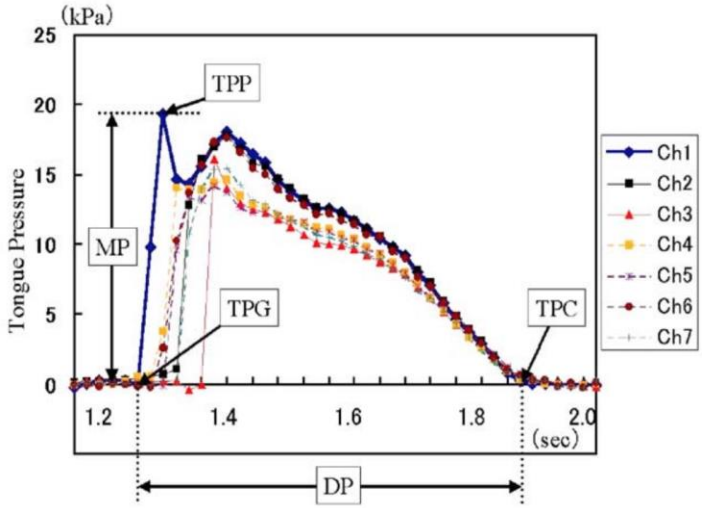

Figure 26 Sample of pressure data recorded from the seven sensors on the palate plate (reproduced as is from [21]).

Specific MP values for each sensor are provided in Figure 27 (reproduced as is from [21]). The maximum magnitude pressure recorded was found at the front section of the tongue Ch 1 at a value of 25.6 (±6.6) KPa. The data provided by this clinical study will be used to determine the appropriate mechanism and power system to ensure similar pressure on the palate. Furthermore, this data supports the importance of continuous pressure on the palate during swallowing as a means of transferring the bolus to the back of the mouth.

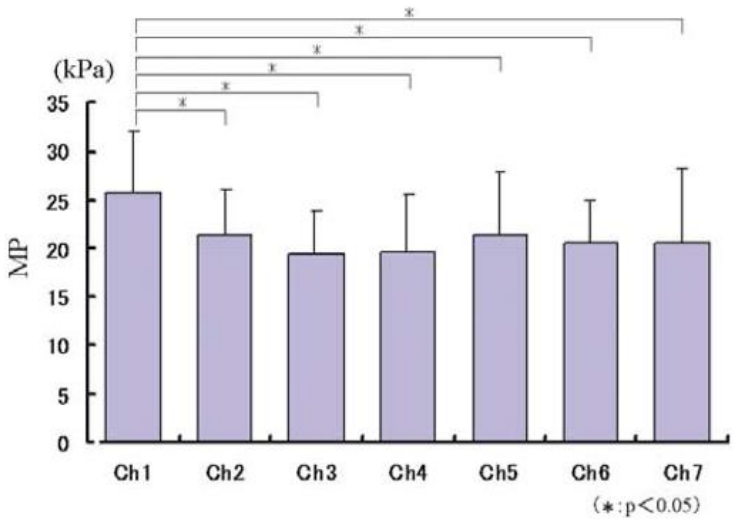

Figure 27 Magnitude Pressure of the tongue on the palate during swallowing (reproduced as is from [21])

Tongue Mechanisms in Industry

The work of Kawamura et al. [22] developed a mechanism seen in Figure 28 (reproduced as is from [23]), known as a multi-degrees of freedom flexible tongue robot. The system is divided into the tip, body and base part of the robot as shown in Figure 29 (reproduced as is from [22]). The tip is composed of an abacus structure for flexibility of motion. The body part is designed to provide a wave caterpillar type motion. The base part is designed to create the upward, downward, left and right motions. For control, the system is composed of a PC, DC motors and encoders. The scale of the assembly is approximately 450 mm tall, 450 mm wide and 450 mm deep. The attributes of this system include stability, independent tongue major functions and the ability to cover the mechanism with a flexible material [22]. The complex motion of the tongue tip section of this mechanism is of interested to this research, as it allows for flexible and controlled motion.

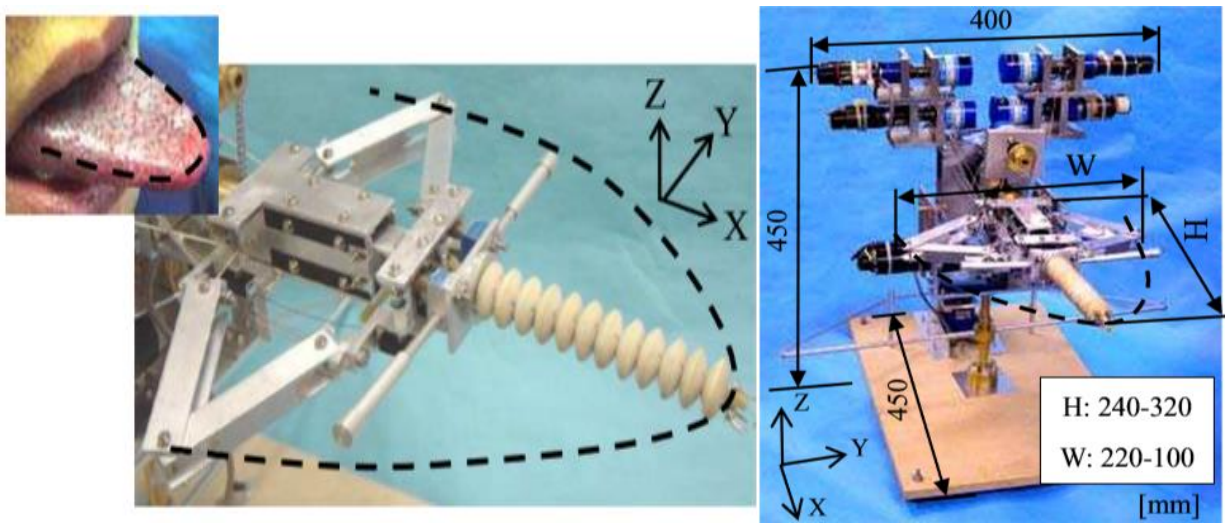

Figure 28 Multi-degrees of freedom tongue robot showing the tip, body and base parts (reproduced as is from [22]).

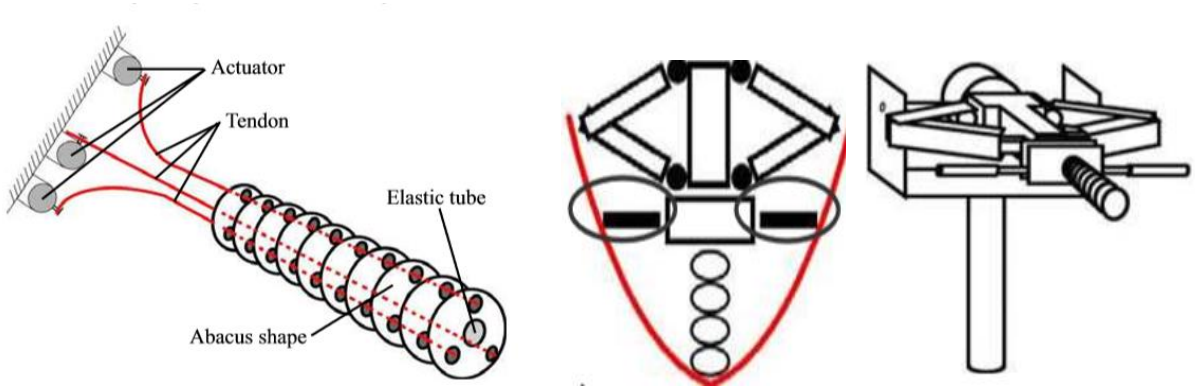

Figure 29 Multi-degrees tongue robot (a) tip, (b) body and (c) base (reproduced as is from [22]).

Another mechanism in industry is known as the pneumatic tongue created by Lu et al. shown in Figure 30 (reproduced as is from [23]). This tongue is made of silicone rubber Eco-flex 00-30 and polydimethylsiloxane material that are formed to incorporate different airways and chambers. Its design was inspired from the PneuNet mechanism theory in which the material elastic properties are used for actuation. Two chambered silicone layers are sealed with a polydimethylsiloxane (PDMS) silicone wrapped layer. Since the sandwiched layers have different elastic properties, they resist axial forces differently, allowing for a bending deflection in the top and bottom layers. This system was developed to recreate the tongue's front section movement including roll up, roll down, elongation, groove, and twist. The size of this system was approximately 34.95 mm in length, 43.70 mm in breadth and 10.66 mm in thickness. The control system is composed of mostly solenoids and pressure sensors [23].

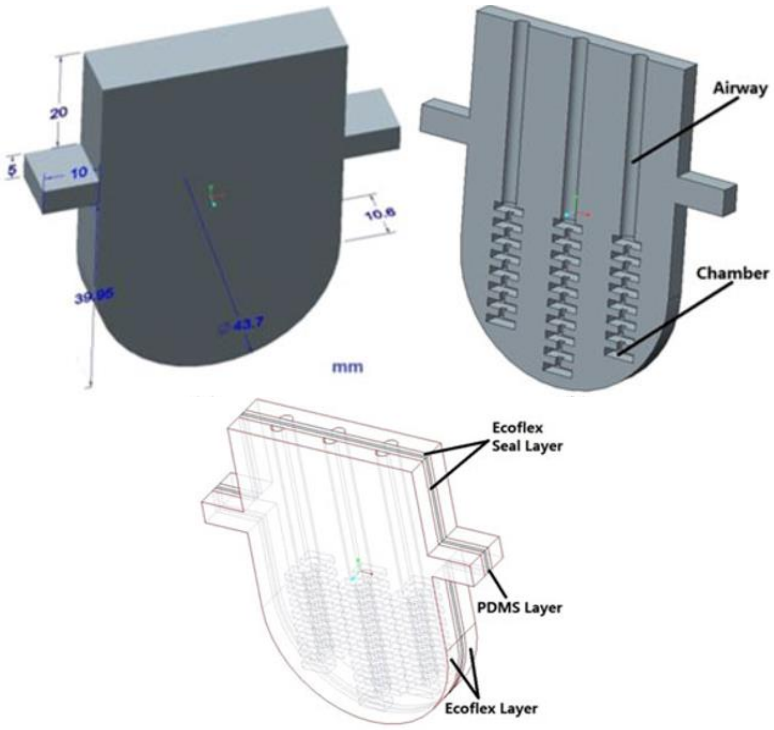

Figure 30 Pneumatic tongue body (reproduced as is from [23]).

The deflection data acquired by this study used input pressures of 21 kPa and positioned tracking points (p1 thru p9) on the tongue as shown in Figure 31 (a) (reproduced as is [23]). These data points were compared with Finite Element Analysis Simulation data and found to have acceptable relative errors of 22% and average error of 11.36% [23]. Figure 31 (b) (represented as is from [23]) shows the comparisons for each recorded section of the tongue. The use of silicone materials for actuation shows attributes of control that will be considered for tongue prosthetic implementation. These may include advantages in miniaturization, pressure control and design.

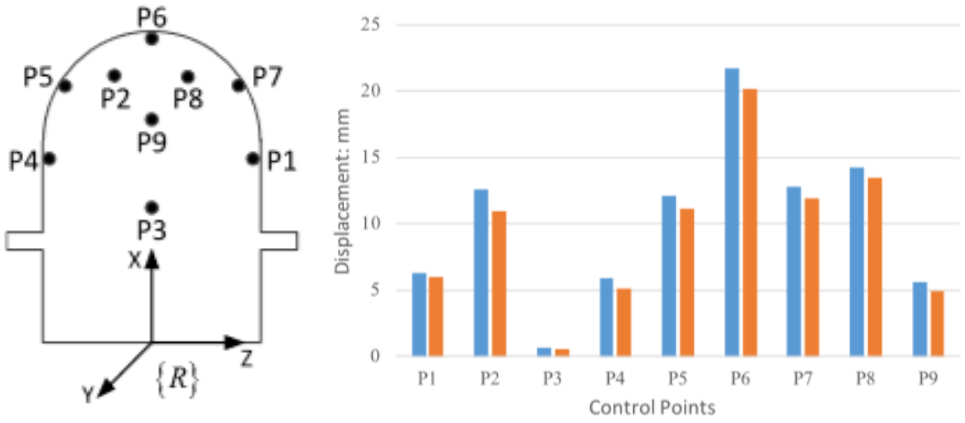

Figure 31 (a) Location of tracking points on robotic tongue and (b) displacement data comparison between experimental and theoretical simulation (reproduced as is from [23]).

Another tongue mechanism in industry can be seen in Figure 32 (reproduced as is from [24]) created by the work of Yamakita et al. at the Takanishi Laboratory in Japan. This tongue mechanism uses shape memory alloys and a displacement amplification system to create miniature actuators that create complex tongue motions. Specifically, the mechanism is divided into three modules known as the Nonlinear viscoelastic module, lock release mechanism and force generator. The force generator provides muscle fiber like contractions. The non-linear viscoelastic module reacts with a change in viscoelasticity from the force. Finally, the lock-release mechanism acts as a muscle relaxer. The size of the actuator is approximately 50 mm in length and 10 mm in diameter. The advantages of this actuator in developing flexible movements was demonstrated in the lab by its implementation into a tongue model shown in Figure 33 (reproduced as is from [24]). Although no complex or specific movements were presented by this prototype, the use of shape memory actuator provides some great attributes to consider in the design of the tongue prototype. For example, the force generator was tested to have a lifting load of 50 grams of force [24]. The combination of several actuators in the design of the prototype may recreate the necessary pressure to push the bolus to the other sections of the tongue.

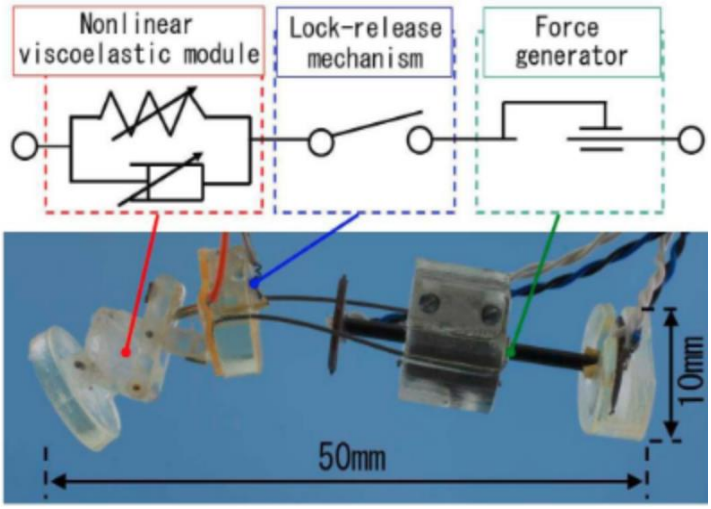

Figure 32 Shape memory miniature actuator attached on a silicon tongue ((reproduced as is from [24]).

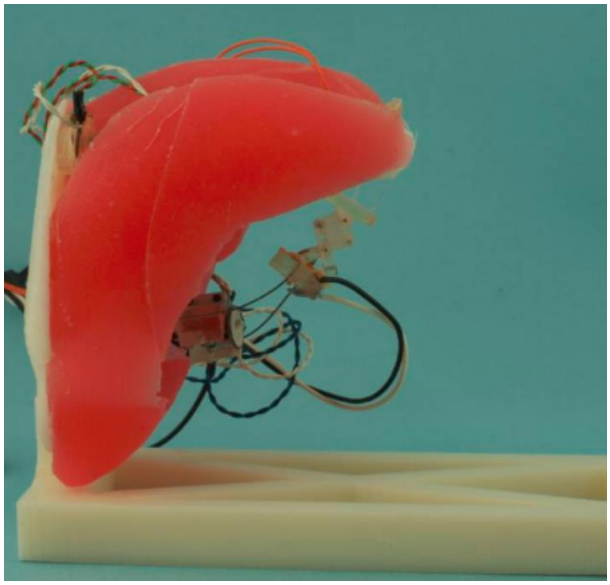

Figure 33 Tongue shaped demonstration model for the miniature actuator (reproduced as is from [24]).

Another mechanism in industry was designed by researchers at Waseda University in Japan [25] and the work of Fukui et al. [26], incorporates three link system for movement of the tongue structure. The mechanism shown in Figure 34 (reproduced as is from [26]) was designed to aid in the formation of vocal sounds through systems like the Waseda Talker, an Anthropomorphic model seen in Figure 35 (reproduced as is from [25]). The linkage tongue mechanism was designed with three degrees of freedom (DOF), one in the tongue tip, two DOF in the tongue blade and two DOF in the tongue body. This study used magnetic resonance imaging of three Japanese vowels being pronounced to develop the appropriate movements of the tongue that would facilitate the

sound created by the Waseda Talker. This three-linkage based mechanism provides an alternative design for a prosthetic tongue. The independent linkages provide the flexibility of timing and deflection adjustments for each section of the tongue.

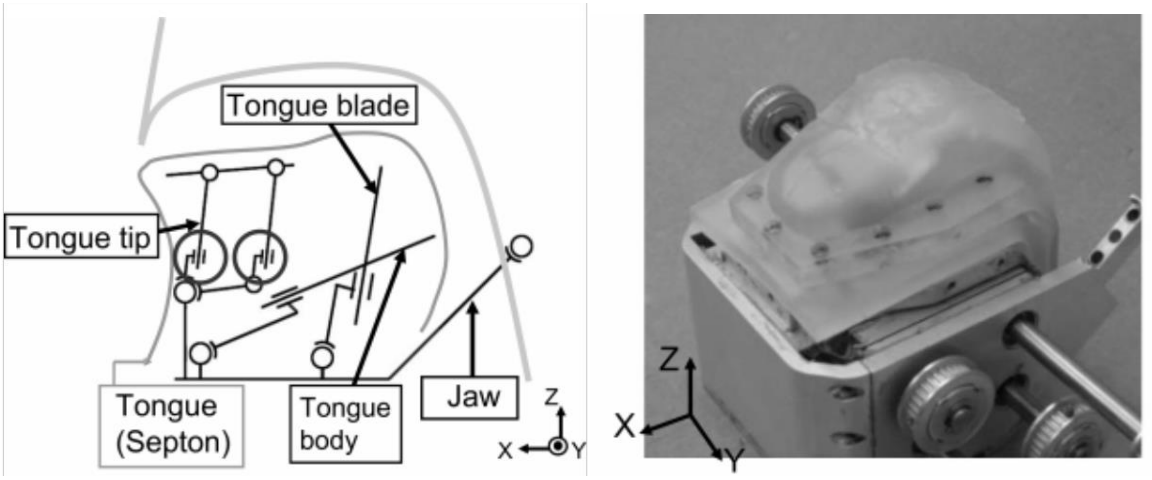

Figure 34 Three link tongue mechanism (reproduced as is from [26]).

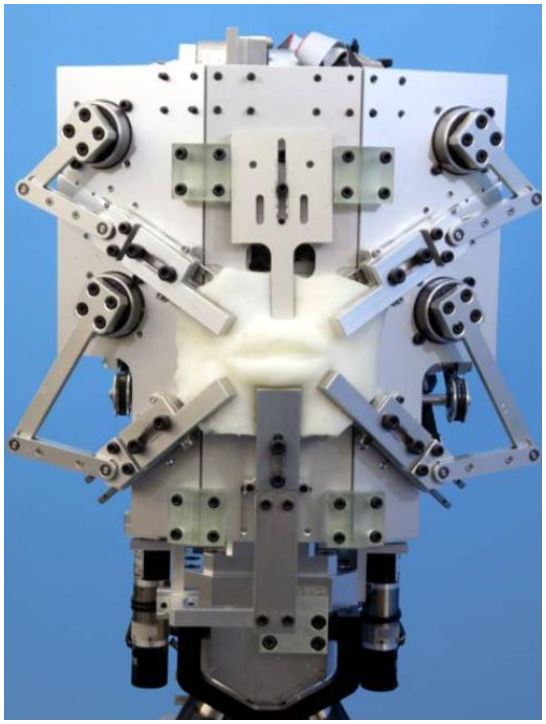

Figure 35 Waseda talking robot (reproduced as is from [25]).

Significance in Various Industries

The results of this research will not only mitigate some of the issues associated with current tongue prosthesis but will also impact research objectives in industries as psychology, educational, pathology and entertainment.

Psychology studies advance the understanding of the human mind by experimenting and gathering data from human subjects**.** A study experimented on what is known as "The Butcher's Tongue Illusion" to understand the multisensory integration of visual, tactile and proprioceptive information [27]. This study utilized a realistic rubber tongue and a mirror system shown in Figure 36 (reproduced as is from [27]) to give the illusion that the participants tongue was indeed the artificial tongue. Through this process, psychologists studied the "visual dominance over the tactile perception" as the tongue was either being touched by a physical item or a light beam [27]. Although the test provided valuable information relating to how humans process touch, it also provided some insight into a significant limitation. The psychologist concluded that the strength of the illusion had a lot to do with the ability of the artificial tongue to react according to the participants real tongue movement. The conclusions made by this study reinforce the need to design a tongue mechanism that esthetically and mechanically can display similar attributes of the human tongue. Furthermore, it can be theorized by analyzing this study, that the static function of the tongue is as important as the reactive movements of tongue and will be considered during the prototype design.

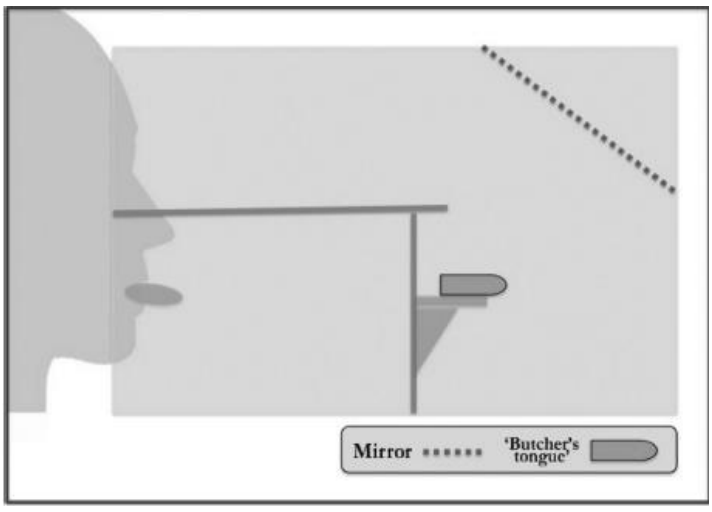

Figure 36 Image depicting "The Butcher's Tongue Illusion" test set up (reproduced as is from [27]).

The educational industry plays an important role in ensuring the competency of the workforce and the advancement of human knowledge. Medical personnel require simulation training to provide exposure to medical procedures that are of high risk for novice practitioners. For these simulations to have the greatest training effect, they must assimilate the movements of a real human beings as closely as possible. A study conducted in the medical field of dentistry, introduced a dental robot shown in Figure 37 (reproduced as is from [28]), that mimics the oral movements of a patient during dental restorations.

Figure 37 Dental robot front view of oral cavity with actuating tongue (reproduced as is from [28]).

One of the capabilities of this robot included the tongue thrust movement that results from patients swallowing or readjusting tongue position during the procedure. This type of movement is concerning to dentist in training as it exposes the patient to great danger from tongue lacerations due to the proximity of the surgical tools. The use of this dental robot, although successful, provided some insight of the performance of the thrusting tongue. The results showed the reactions to the tongue thrust to be lower due to the dentist in training inability to either "notice the tongue movement or simply disregarding it" [28]. When analyzing this closely, it can be argued that the student's inability to "notice" the movement of the tongue may be directly associated with how realistic the movement of the tongue was and the location within the mouth that the restorative work was being performed. Due to this study, the design of the tongue prototype, will take into consideration the lateral interaction of the tongue during actuation. This may be an important consideration to make to ensure that the dimensions of the tongue do no conflict with the dimensions of the oral cavity during movement.

The field of pathology has furthered humans understanding of our vocal capabilities. Due to the limitations of speech research on live subjects, it has been imperative to utilize technology to further understand and resolve some of the ongoing questions related to speech. A team at the University of Sheffield, UK, studying the energy invested in speech, created an animatronic model called “Anton” shown in Figure 38 (reproduced as is from [29]) that incorporates a mechanical tongue and vocal tract system [29]. The design of the tongue was composed of a mesh system attached by filament wires and control by electric motors.

The approaches taken in this study, which they believe to differ from other studies, is to model the components structure based on human physiology instead of functionality. The intent of this research was to utilize the physiology and anatomical movement of the tongue to artificially recreate sounds and measure the energy consumption utilized in the process. Although the system design met the research intent, it is evident its performance was reliant on the technological advancements available at the time of the research. This study in general brings up the importance of considering the anatomical aspects of the tongue when creating a prosthetic device. The tongue surface geometry will play a large role in assisting the deglutition process. Furthermore, the filament-based mechanism is an interesting design and may be used as an exploratory step in the development of the tongue prosthetic.

Figure 38 Anton animatronic model oral cavity view of actuating tongue (reproduced as is from [29]).

Finally, the creative industries have also benefited from the advancement of mechatronic technology. The formulation of artistic ideas to convey specific or abstract messages is a passion for mechanic sculpture Server Demirtas [30]. His contemporary Istanbul sculpture presentation, known as the Koro/Choir shown in Figure 39 (reproduced as is from [30]), integrated three animatronic faces that are programed to continuously simulate the human motion of licking [30].

This simulated motion is very simplistic in design and can be more associated with the forward and back motion of the tongue. Even in its simplistic form, the depiction of such relatable motions invokes a very individual and subjective emotion, increasing the effectiveness of the artist expression. It is evident that the use of a more sophisticated tongue could provide even greater responses that would certainly enrich the arts aficionado experience and the enjoyment of the art.

The next chapter will describe in detail the process of selecting the foundational design for the prototype and the supporting arguments for such selection.

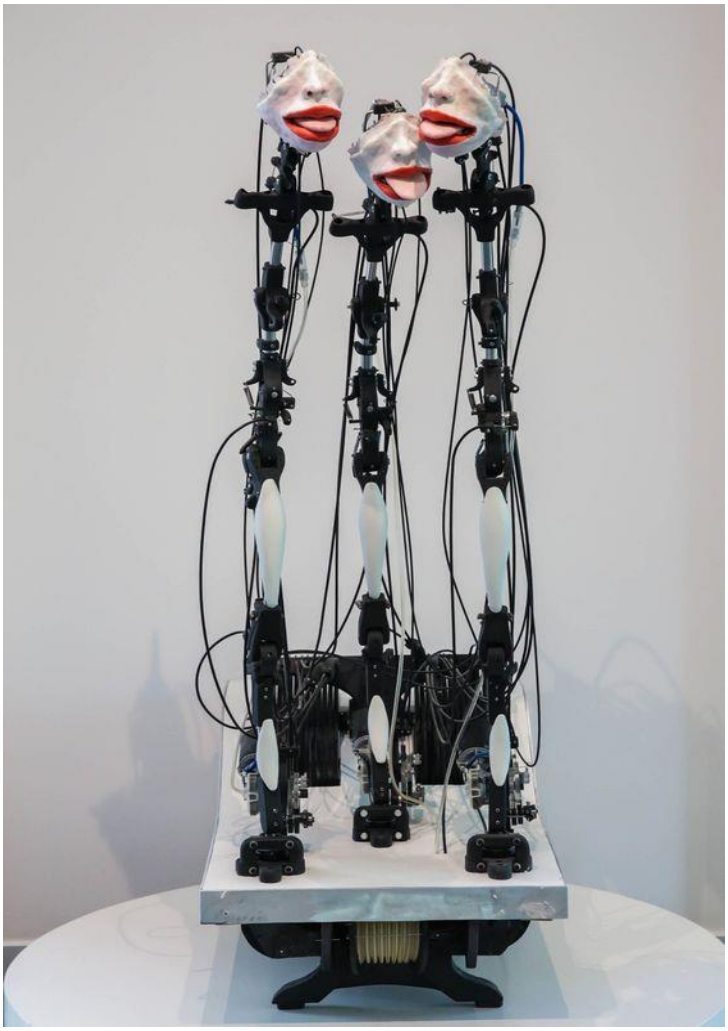

Figure 39 Choir mechanical sculpture of licking faces (reproduced as is from [30]).

V. Actuation Selection

This chapter introduces the prototype design process by discussing the mechanism type selection matrix, the selected foundational design and the governing equations of the design. Justifications and applications of the chosen design are provided in detail.

Mechanism Type Selection Matrix

To select the mechanism that will be used as a foundational design for the tongue prototype, a design decision matrix was created as show in Table 1. The intent of this decision matrix is to, based on the information provided in the literature review, score each mechanism on its foreseeable ability to meet the functional requirements and attributes of the tongue prototype. These requirements and attributes include swallowing movement, swallowing pressure, biological adaptability, miniaturization, manufacturability and low cost. Additional conclusions were made on each mechanism relating to several factors. First, several systems including the multi-degrees tongue robot and linkage mechanisms, use no clinical data of the human tongue to realize the respective motions. Secondly, several mechanisms were designed to recreated speaking sounds and not for recreating the swallowing motion. Finally, except for PneuNets, the mechanisms were not designed with scalability in mind. Several scores were given for this attribute based on the theorized possibility of scalability based on the design details provided by the scholarly articles.

Table 1 Decision matrix table.

Mechanisms	Swallowing Movement	Swallowing Pressure	Biological Adaptability	Miniaturization	Manufacturability	Low Cost	Score
Multi-Degrees Tongue Robot	50	100	50	20	20	20	49
PneuNet Tongue Actuator	80	100	100	50	80	50	74
Shape Memory	50	100	20	20	20	50	40
Three Linkage	80	80	100	50	50	50	67
Filament Anatomical	80	50	100	50	80	50	64

Based on the scores developed on the decision matrix process, it was determined, that the mechanical system that provided the greatest foreseeable attributes to the prosthetic design would be the PneuNet Tongue Actuator.

The mechanism chosen was first introduced in industry by a group of Harvard students in the year 2014 [31]. PneuNets have many attributes that can be of great use for developing a prosthetic tongue. First, silicone grade materials as HTV and RTV are already used in maxillofacial static prosthetic systems due to their excellent tear and tensile strength of

approximately 587 MPa [32]. Secondly, silicone materials provide excellent thermal, color and chemical stability allowing for better adaptability in biological environments [32]. Thirdly, the fluid source for actuation is readily available in the oral cavity and can be easily recycled. Finally, the manufacturing process can be achieved through the use accessible resources as pneumatic air and 3D printing systems.

Selected Foundational Design

A specific foundational design used extensively in the prototype process relates to the work of Shepperd et al. [33] in Multigait robots and the work of Jiawei et al. [34] in the untethered robot. The theory behind the design relies on the adhesion of two dissimilar materials with different strain properties. As shown in Figure 40 (reproduced as is from [33]), Layer 1 consist of an extensible elastomer with series of air chambers for deformation. Layer 2 consist of a non-elastic material that limits the extension of the bottom surface of the robot. Using pneumatic air, each chamber is pressurized allowing for the deflection of the elastic layer in the axial direction. By controlling this pressure and separating the chamber sections of the assembly, the multigait robot can be controlled by the operator to perform specific motions.

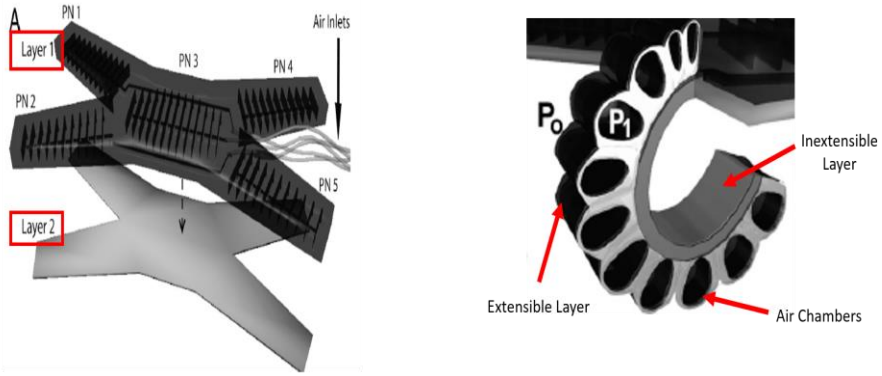

Figure 40 Multigait Robot (a) assembly and (b) tentacle detail view (reproduced as is from [33]).

Design Governing Equations

The theory behind the bending deflection of the multigait robot can be explain through simple equations provided in the work of Onal et al. [35] as shown in Equation 1 (a) Axial Stress and (b) Total Axial Stress Deformation. The stress (σ_x) induced in the chambers is based on the Pressure (P), height of the chamber (h_c) and height of the material (h_t). The total axial deformation (δ_x) of the actuator is based on the product of the non-linear strain (ε_x), length of the air chambers

(l_c), individual chamber stress (σ_x) and number of chambers (n). This total axial deformation translates to the bending deflection of the upper chambered layer.

$$\sigma_x = P\frac{h_c}{h_t - h_c} \qquad \delta_x = n\imath_c\mathcal{E}_x(\sigma_x) \tag{1}$$

To better visualize these equations, a simplified mold structure with associated parameters is shown in Figure 41 .

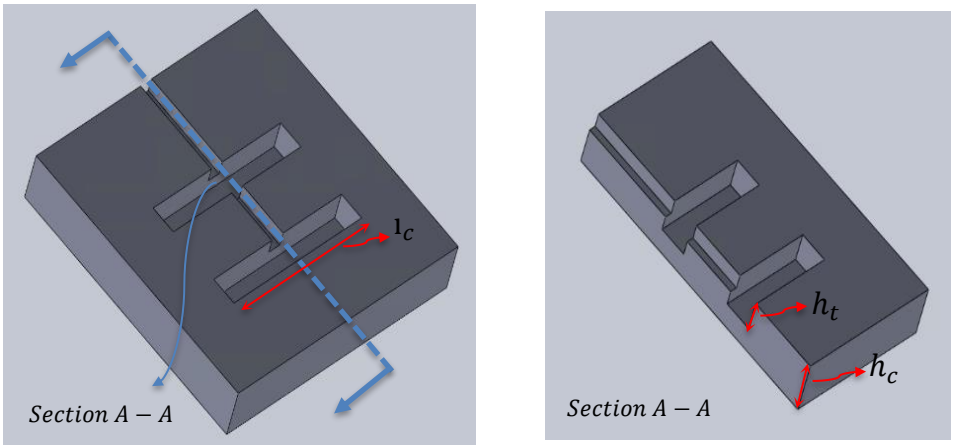

Figure 41 Simplified PneuNet mold structure (a) assembly and (b) Section A-A detail.

Another governing equation for the design of silicone actuators can be described by the work of Sun et al. [36]. The theory behind Equation 2 assumes that to develop a torque (T_c) at a specific point on a soft pneumatic actuator, the differences in internal and external forces must be of different magnitudes. These internal forces include variables as the cross-sectional area of the inflated air chamber (A_p), the cross sectional area of the wall (A_w), the input pressure (ΔP), the stress normal to A_w (σ), the moment arm (a) the height of the inflated chamber (h) and the external force blocking further deformation (F). Figure 42 provides a visual representation of the Forces, Torque and the variables previously mentioned.

$$T_c = A_p\Delta P\frac{h}{2} - A_w\sigma h - aF = 0 \tag{2}$$

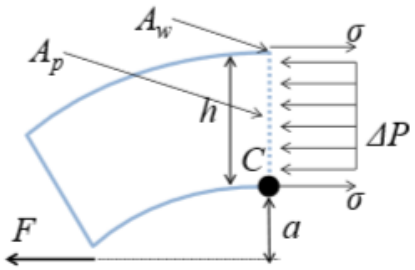

Figure 42 Forces and Torque acting on the bending soft pneumatic actuator (reproduced as is from [36]).

These governing equations have been fundamental in the development of PneuNet Actuating Robots as the one shown in Figure 43 (reproduced as is from [35]). Measuring 80 mm in diameter and 63 mm length, this mobile robot uses Fluidic Elastomer actuators, attached to the circumference of the cylindrical structure, to exert a rolling force.

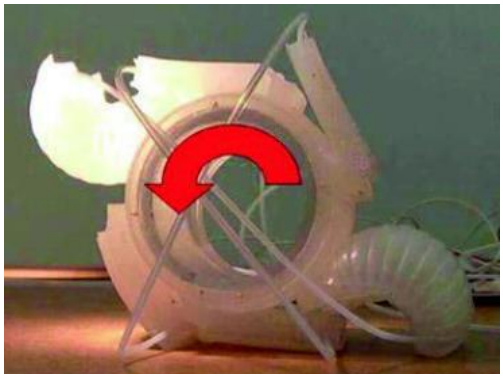

Figure 43 Rolling mobile robot with PneuNet actuators (reproduced as is from [29]).

A more relatable application of PneuNet actuators can be seen in the work of Deimel et al. [37] in the underactuated robotic hand shown in

Figure 44 (reproduced as is from [37]). The robotic hand is composed of seven PneuNet actuators designed to perform complex motions when holding different types of items. As seen in Figure 45 (reproduced as is from [37]), the hand robot is holding a rolling pin that weights 0.54 kg. The intent of the work developing this robotic hand is to demonstrate its effectiveness is providing various grasp postures and behavior with “relatively simple control” [37].

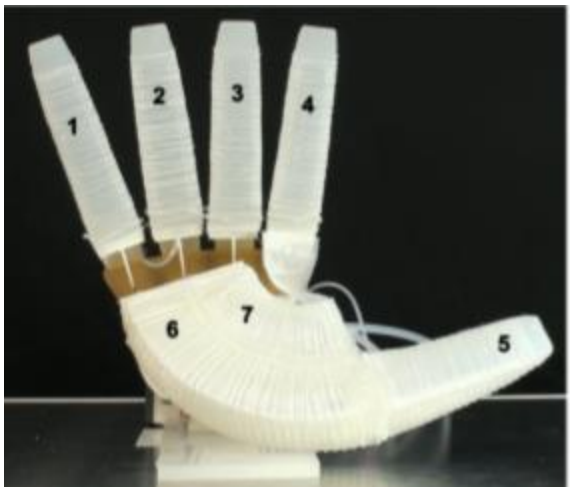

Figure 44 Underactuated robotic hand for dexterous grasping (reproduced as is from [37]).

Figure 45 Underactuated robotic hand holding a rolling pin (reproduced as is from [37]).

Manufacture of PneuNets

The general process for manufacturing PneuNets can be described in the flow chart shown in Figure 46. The process begins by first developing the mold using a solid modeling software. These molds are typically composed of a chambered section and a solid section. This design must then be physically created using various means that may include Fused Filament Fabrication, Casting and Laster cutting. Once the molds have been created, the molds are filled with a silicone-based mixture and left to cure to the silicone's manufacturers specifications. Once the silicone has hardened, the layers of molded silicone are removed from the mold and inspected for any defects. If no defects are found on the matting surfaces, the layers can then be adhered together using silicone-based adhesives. The same mixture used to create the silicone actuators can be used to adhere both layers. Once the layers adhesive mixture has cured, the silicone actuator can now be

punctured at the respective locations to insert the inlet tubing for pressurized air. The next chapter will describe in detail the process taken to manufacture and develop prototype design iterations.

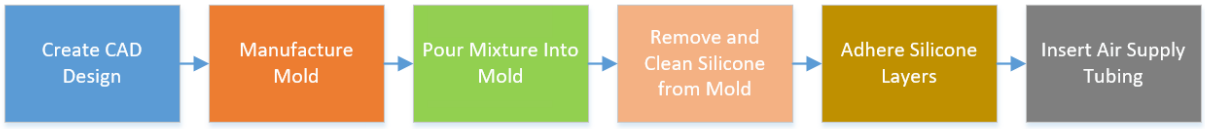

Figure 46 Flow chart showing the typical processes involved in manufacturing PneuNet actuators.

VI. Design and Manufacture of PneuNet Actuator Tongue

This chapter introduces the materials and manufacture process selected to develop the molds for the PneuNet actuator tongue. It also provides the design iterations taken to learn and modify existing designs to meet the motion requirements of the tongue.

Materials and Manufacturing Process

The method chosen for manufacturing the molds for the PneuNet actuators was Fused Filament Fabrication (FFF). This method was chosen for several advantageous reasons. First, FFF can be accomplished at relatively low costs. An FFF system, known as Rep Rap Guru as the one shown in Figure 47 (reproduced as is from [38]), is approximately $300 dollars. The required filament of about 280 m in length can be purchased for about $40 dollars per roll. This allows numerous prints to be created before purchasing a new roll. Secondly, the information available for FFF systems has increased largely in the online forums. From manufacture support sites to hobby blogs posts, common problems that are encountered during the printing process can be quickly resolved. Finally, the safety operation of FFF systems allows for long hour printing to be accomplished without supervision. All these reasons combined, make FFF a very versatile system to use in the iterative design process of this research.

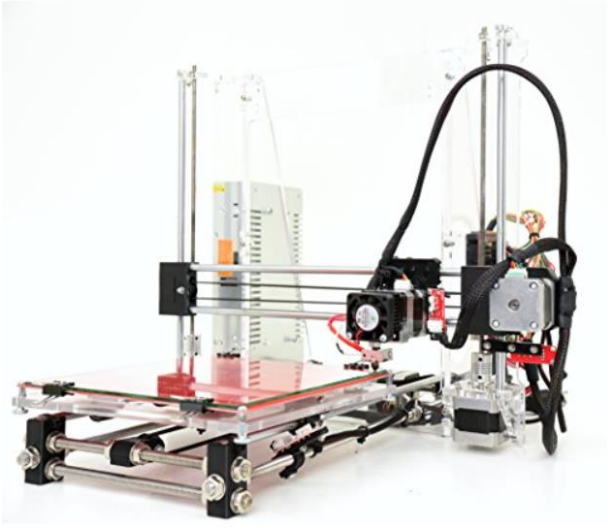

Figure 47 Rep Guru 3D printer V1 model (reproduced as is from [38]).

Initial Trial Iteration

The prototype manufacturing process began by first trying to replicate the work performed by Jiawei et al. [34] related to the untethered robot. Using SolidWorks 3D models provided by Jiawei et al. [34], STL files were created by a simple change in format in SolidWorks. Using slicing open source software as Slicer3r [44], the STL files were sliced to the printing parameters selected and transferred into g-code format. This format was then sent to the printing software on the Rep Rap Guru FFF printer for printing. Polylactic Acid material (PLA) was used as a primary printing material in this research. Extruder temperatures of 210 degrees C and printing base temperatures of 55 degrees C were used for the 1.75 mm PLA filament. Additional printing parameters used for optimizing the printing quality are provided in Appendix A.

The untethered robot mold assembly printed is shown in Figure 48 and it is composed of an upper layer molds (chambered and surface design) and lower mold. As noted, the pressurized air is supplied from the inlet to the different sections of the robot through short chamber spaces created by the molds. The larger mold chambers are connected to these short chambers which will be the major surface for the pressurized air to exert force on.

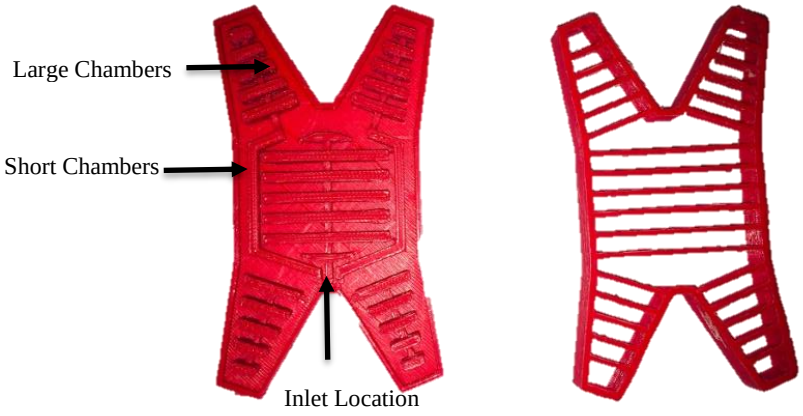

Figure 48 Untethered robot PLA molds.

After printing, the molds were trimmed to ensure tight fit and clean edges. The silicone 1:1 ratio mixture of Eco-flex 00-30 A and B is poured into the molds until the mixture reaches the top edge as shown in Figure 49. After approximately eight hours of curing at room temperature, the silicone structure is ready to be removed.

Figure 49 Untethered robot silicone mold pour.

The resulting silicone structures shown in Figure 50and associated inlet tubing were then adhered as a single assembly with Silicone RTV and left to cure for approximately 24 hours.

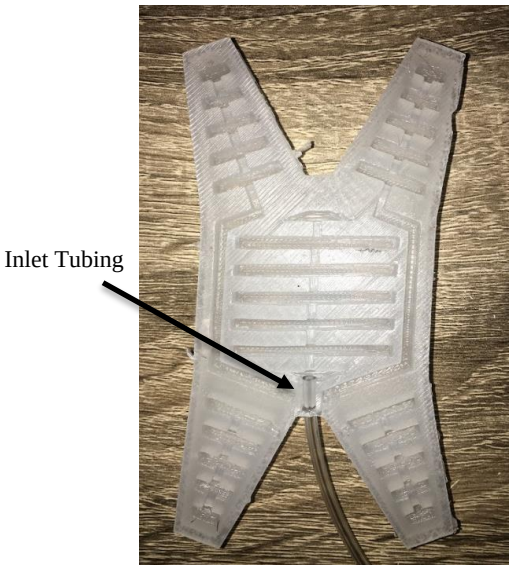

Figure 50 Resulting mold silicone structure and inlet tubing.

Using three 100 ml type syringes shown in Figure 51, compressed air was manually supplied to the respective inlet hoses for actuation testing purposes.

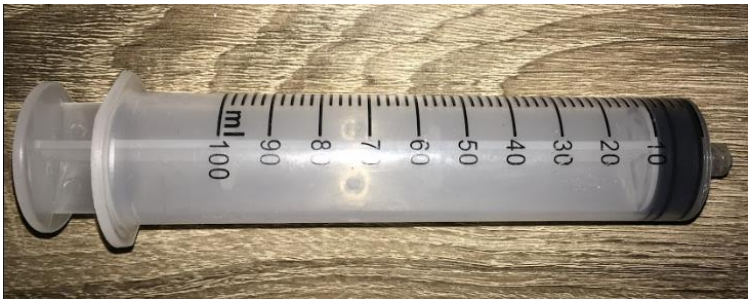

Figure 51 A 100 ml syringe used for manually actuating robot.

The testing process of the untethered robot resulted in the unsuccessful actuation of the robot. It was determined after destructive inspection of the cured assembly that many manufacturing defects, contributed to the failure of this assembly. First, the fit of the top and surface geometry molds played a large role in the leakage of the silicone mixture. As shown in Figure 52, clearance between the molds allowed for the poured silicone to seep out, thereby reducing the thickness of the upper layer. This leakage rendered thin actuator walls which would easily reach the material yield point under pressure. An image of the thin top walls is provided in Figure 53.

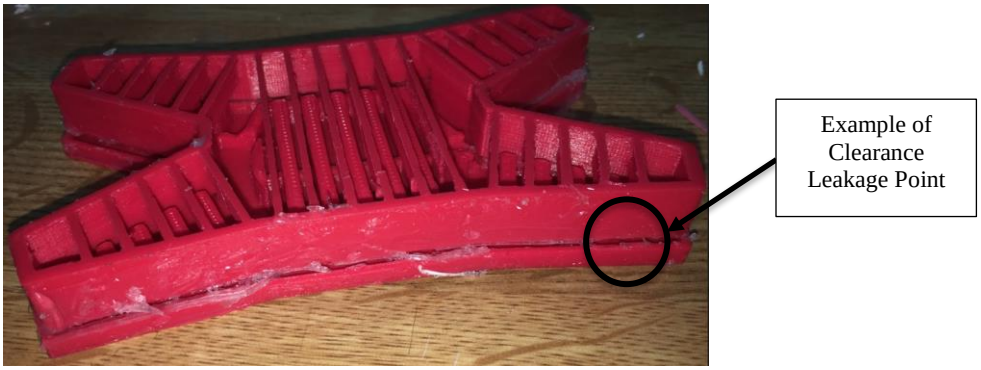

Figure 52 Untethered robot molds with areas of clearance.

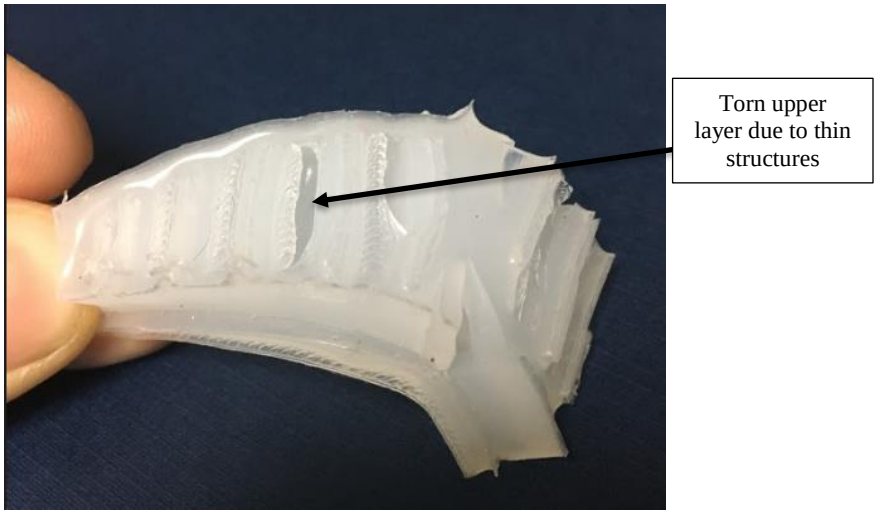

Figure 53 Untethered robot failure of top layer walls on tentacle.

A second issue found is related to leakage of air in the actuator assembly. This was a major contributor to the lack of actuation from several sections of the Untethered robot. In an unsuccessful attempt to seal the inlet point of the actuator due to excessive air leakage, RTV was used as shown in Figure 54.

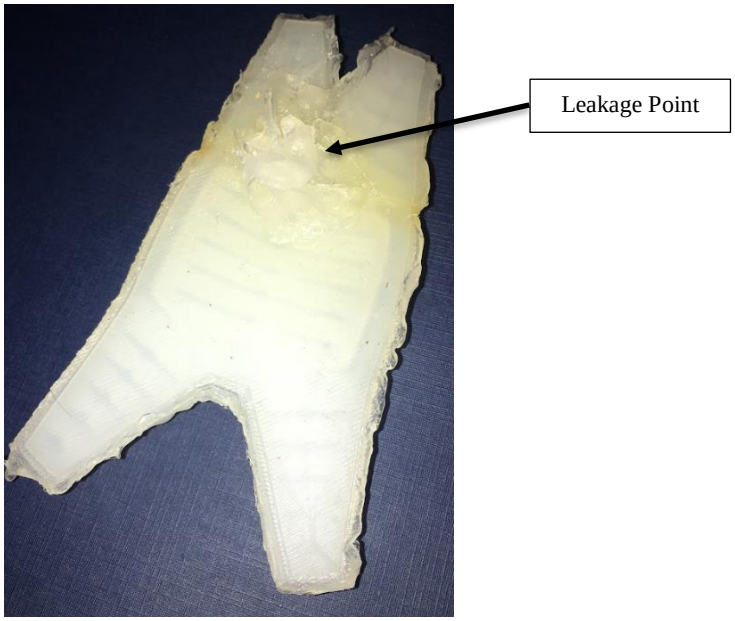

Figure 54 Untethered robot inlet leakage attempted repair.

In retrospect, the issues encountered by this trial iteration disclose the lack of detailed open source information in the development of PneuNet systems. Although general aspects of the manufacturing process are mentioned in many scholarly articles, the minor details of the molding

process have been identified in this process as the limiting factor in successfully and consistently replicating actuators as the one mentioned above.

Incorporation of Initial Trial Findings into Tongue Design

Based on the information gathered in the literature review and the learned outcomes of the Untethered robot trial run, the first tongue shaped iteration was developed. As shown in the in Figure 55 (a), the CAD models of the proposed tongue included the bottom layer mold top layer mold and surface geometry mold. The middle mold was divided into three areas of the tongue for actuation. These areas included, front, middle and back to match the T2, T3, and T4 points of the tongue provided in the literature review kinematic data as shown in Figure 55 (b) (reproduced as is from [20]). The design did not use T1 point due to the noted inconsistency and variability of the data gathered by researchers.

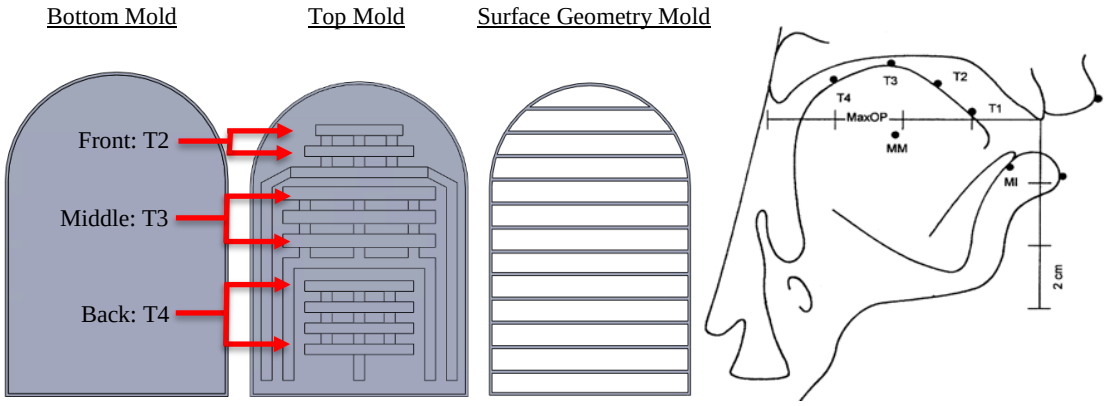

Figure 55 First iteration (a) showing the bottom mold, top mold and the surface geometry mold and (b) Position of pellets from clinical study (reproduced as is from [20]).

This first tongue design followed similar design features as the Untethered robot in which air chambers are developed in the top layer along with air passages as shown in Figure 56. The air passages are routed to the to the sides and towards the back of the tongue. This was done to allow for a single point of input and to allow for continuous lengths of air chambers. Furthermore, based on the air leakage issues experience in the Untethered robot, focus was placed on providing enough space between inlet points to reduce the possibility of air leakage during input tubing installation. In addition, each section of air chambers is connected with three air passage columns to evenly distribute the supply air. Also, the top and surface geometry molds were designed to fit tightly

together for the purpose of reducing the silicone mixture leakage encountered in the Untethered robot trial iteration.

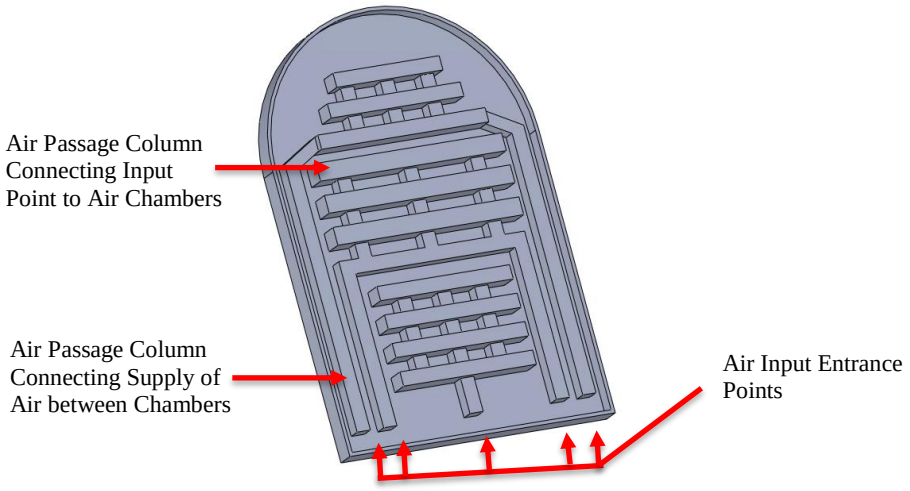

Figure 56 First iteration design parameters.

The CAD models were 3D printed using FFF. Figure 57 First tongue iteration 3D printed molds including (a) bottom layer, (b) top layer and (c) surface geometry layer. Figure 57 provides the resulting 3D printed models that include (a) bottom layer, (b) top layer and (c) surface geometry layer.

Figure 57 First tongue iteration 3D printed molds including (a) bottom layer, (b) top layer and (c) surface geometry layer.

Once the printing models were assembled, the silicone mixture was poured in. During this silicone pour process, the prototype molds encountered similar issues with silicone mixture seepage between the top and surface geometry molds. To resolve this issue, painters' blue tape was wrapped around the mold, as shown in Figure 58, to reduce leakage to acceptable levels.

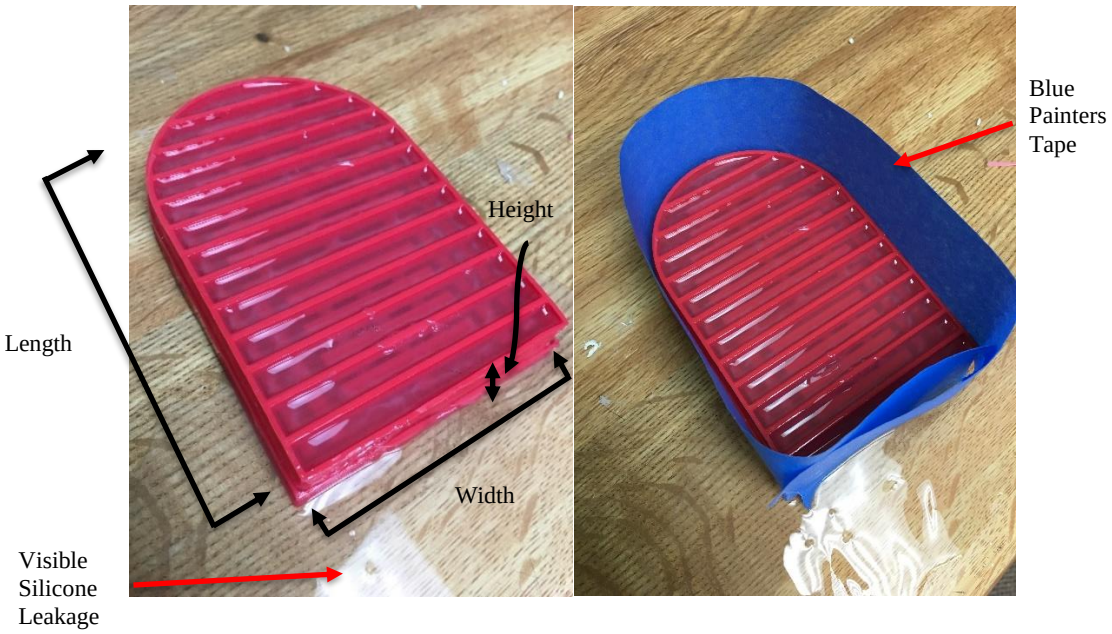

Figure 58 First iteration (a) mold leakage and (b) mitigating solution.

The resulting silicone layers shown in Figure 59, were adhered together with silicone RTV and allowed to cure for 24 hours. The input tubing was then installed at the locations provided and sealed with additional silicone RTV. Table 2 provides dimensions of the CAD model, printed mold, and silicone actuator resulting structure.

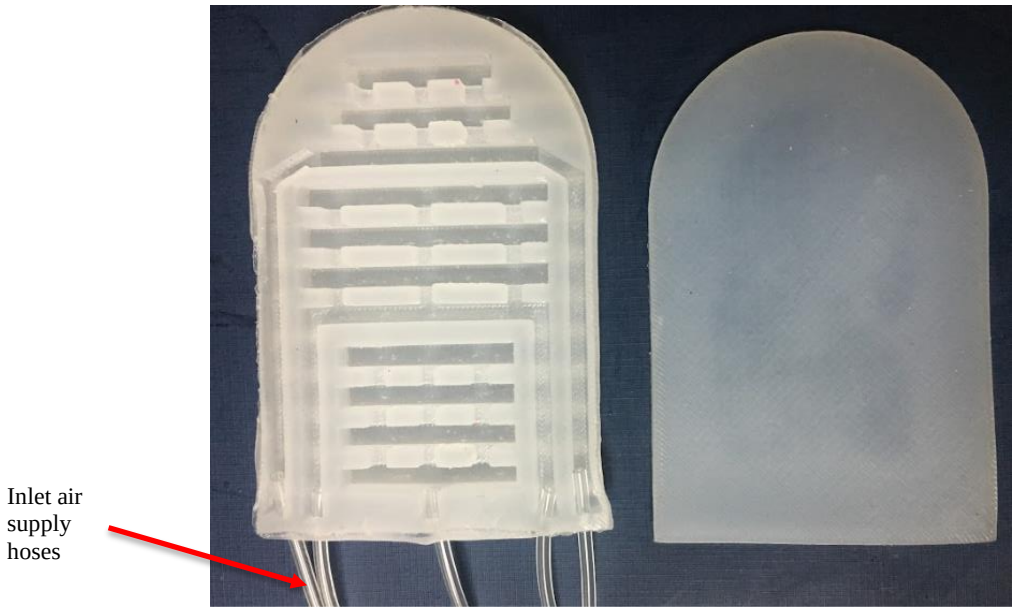

Figure 59 Resulting Silicone Layers

Table 2 First Iteration Manufacturing Dimensions

Format	**Overall** **L x W x H** **(inch)**	**Air Chamber Row** **L x W x H** **(middle)** **(inch)**	**Air Passage Column** **L x W x H** **(middle)** **(inch)**	**Assembly Weight** **(ounce)**
CAD Model	3.94 x 2.9 x 0.3	2.0 x .13 x .19	0.1 x 0.1x 0.15	N/A
PLA Mold	4.5 x 3.0 x 0.50	2.2 x 0.205 x .3	0.15 x .17 x .18	2.2
Silicone Actuator	4.6 x 2.97 x 0.52	2.2 x 0.23	0.17 x 0.18 x .16	3.9

The manual test of this actuator, using three 100 ml syringes, successfully verified the theoretical wave like motion of the tongue, starting from the front to the back of the actuator as shown in Figure 60. This motion begins with step one, static state. Step two, tip up motion. Step three, deflection of the front section of the tongue. Step four, deflection of the middle of the tongue. Step five, deflection of the back section of the tongue and step six, original static position.

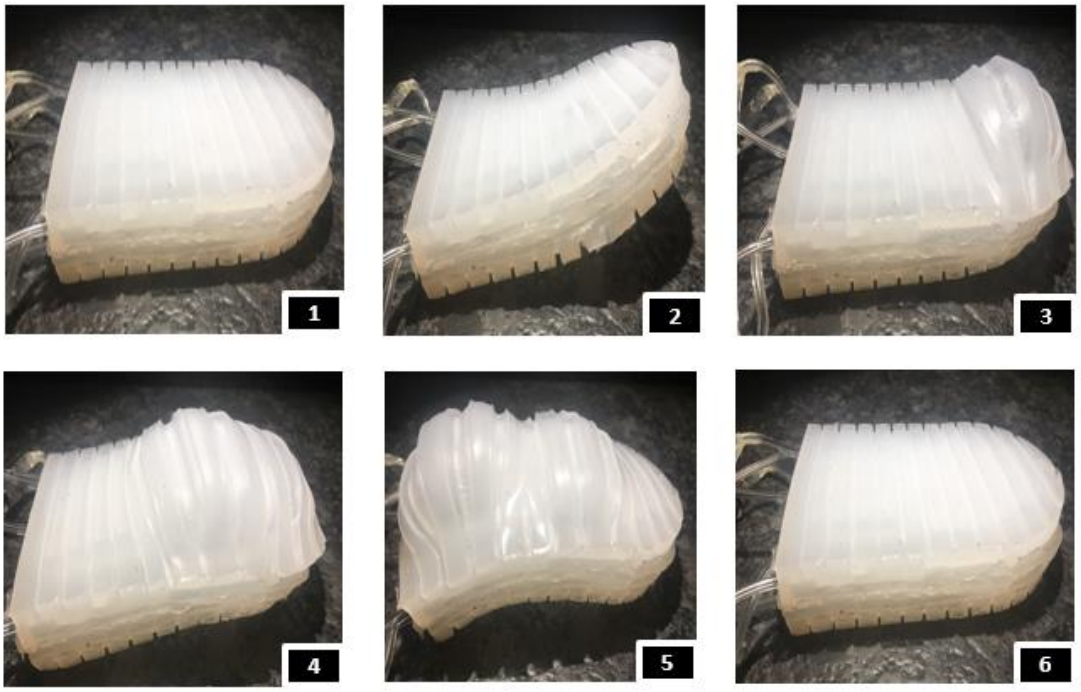

Figure 60 Tongue prototype first iteration recorded motion.

The overall analysis of this first tongue iteration determined a few manufacturing aspects to consider for future iterations. First, when comparing the values shown in Table 2, it is theorized that the slicing software was increasing the dimensions of the molds. Secondly, uncontrolled shrinkage of the parts during printing, created additional inconsistent dimension changes to the parts. This was apparent during the assembly of the top and surface geometry mold by the

excessive clearance of the parts. This was found to be the major contributor to silicone mixture seepage during the silicone structure manufacturing process.

The information gathered in this iteration, realized the feasibility to manufacture silicone PneuNets with low cost equipment. The wave like movement developed in this iteration, shows promise of achieving the swallowing motion in future iterations.

Miniaturization Iterations

For the second mold design iteration, miniaturization of the first iteration was attempted. In the first iteration, the scale on the CAD models ware reduced to a smaller scale. In an attempt to print the designed molds, printing quality issues were encountered. The printing quality of the printer made it difficult to print the air chambers of the mold at the required scale. Despite this issue, further attempts were made to continue to use 3D printing as a means of manufacturing molds due to its low cost and exploratory aspect. A satisfactory solution to quality was developed that involved reducing the layer thickness and the extrusion multiplier. An image of the end result of these adjustments is shown in Figure 61.

Figure 61 Mold design for the second iteration of the prototype (a) CAD model (b) FFF printed mold

Finally, since no adjustments were made to the number of chambers and the spacing between sections, the mold scale made it difficult to remove the silicone structure without tearing the chamber dividing walls. Figure 62 provides a detail view of the torn areas of the silicone structure design.

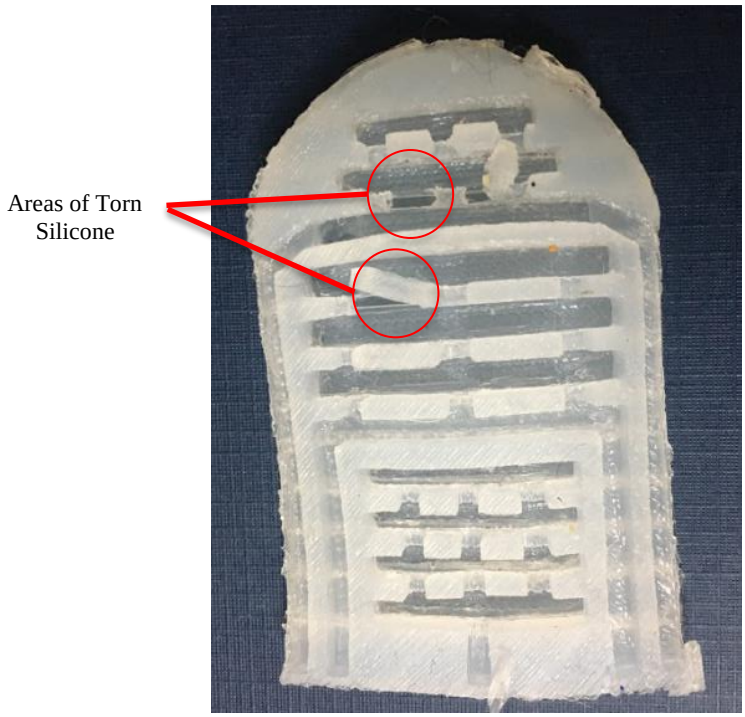

Figure 62 Silicone design for the second iteration of the prototype.

The dimensions for this iteration are provided in Table 3.

Table 3 Second Iteration Manufacturing Dimensions

Format	**Overall** **L x W x H** **(inch)**	**Air Chamber Row** **L x W x H** **(middle)** **(inch)**	**Air Passage Column L x W x H** **(middle)** **(inch)**	**Assembly Weight** **(ounce)**
CAD Model	2.9 x 1.95 x 0.2	1.4 x 0.13 x 0.19	0.1 x 0.1x 0.1	N/A
PLA Mold	2.7 x 1.8 x 0.17	1.3 x 0.125 x 0.18	0.1 x 0.07 x 0.1	0.4
Silicone Actuator	2.6 x 1.7 x 0.16	1.3 x .125 x 0.14	0.1 x 0.07 x 0.1	0.3

After several attempts resulted in torn sections of the silicone actuator, it was decided that further iterations were necessary to achieve a functioning silicone structure. This iteration showed the complexity in small scale manufacturing of PneuNets actuators. Furthermore, based on the data provided in Table 3, the slicer software seemed to work as intended. The parts printed did experience shrinkage of about 0.2 inches from the dimensions of the CAD model. Finally, it was decided through this iteration that increasing the space between chambers and reducing the air supply passages will be necessary to provide stability of the silicone structure to reduce tearing.

The third iteration of the prototype focused on resolving the issues found in the second iteration. A reduction in the number of air chambers was made to ensure enough wall thickness. This would also aid in preventing leakage between chambers and adhesion to bottom layer. With these new changes, the silicone mold structures were developed following similar printing processes. An image of the third iteration molds is provided in Figure 63.

Figure 63 Mold design for the third iteration of the prototype.

Following similar silicone pour processes, the third iteration silicone molds were developed as shown in Figure 64. The silicone structure was assembled in the same process as the previous iterations. Due to the size of the center walls, careful application of the RTV mixture was achieved to ensure the air chamber and supply passages were not obstructed.

Figure 64 Silicone structure for the third iteration of the prototype.

The dimensions for this iteration are provided in Table 4 .

Table 4 Third Iteration Manufacturing Dimensions

Format	**Overall** **L x W x H** **(inch)**	**Air Chamber Row** **L x W x H** **(middle)** **(inch)**	**Air Passage Column L x W x H** **(middle)** **(inch)**	**Assembly Weight** **(ounce)**
CAD Model	3.2 x 2.46 x 0.3	1.5 x 0.1 x 0.1	0.2 x 0.1x 0.08	N/A
PLA Mold	2.6 x 2.0 x 0.25	1.2 x 0.12 x 0.12	0.15 x 0.12 x 0.09	0.4
Silicone Actuator	2.4 x 1.8 x 0.24	1.18 x 0.07 x 0.08	0.15 x 0.09 x 0.07	0.4

During the testing process, a familiar issue experienced in the Untethered robot emerged. Leakage around the inlet tubing became increasingly difficult to contain. This was theorized to be associated with the number of inlet locations, the space provided to attach the tubing to the actuator and the challenges in attaching two dissimilar materials. Furthermore, the scalability of the molds, limits the space available for routing the input air passages. The space provided and location of leakage can be seen in Figure 65.

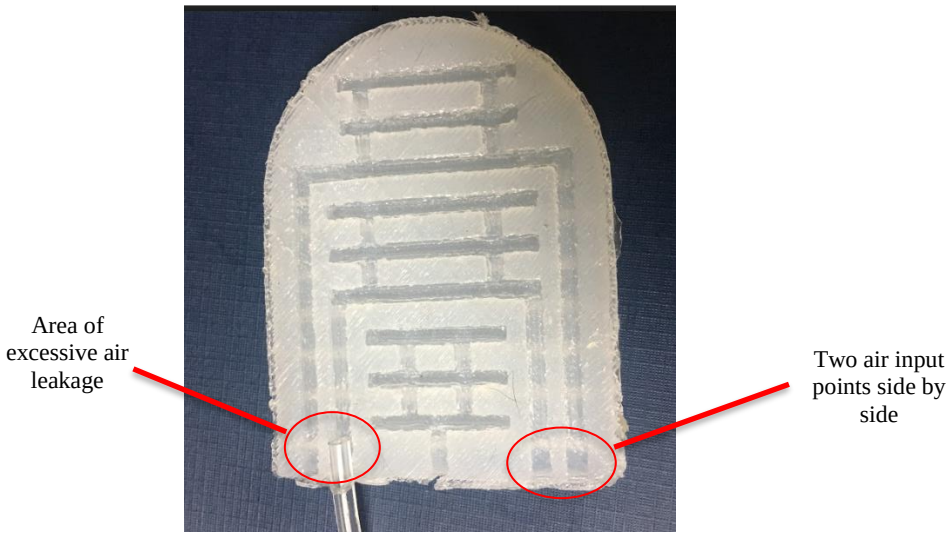

Figure 65 Leakage location and space provide for input air passages.

The information gathered in this iteration provided additional insights into the complexity of manufacturing of small scale PneuNets systems. This iteration experienced similar shrinkage of 3D printed parts as the last two iterations as shown in Table 4. Also, due to excessive input air leakage around air passages, the resulting actuator could not function. It was determined through

this iteration that reducing the input air passages by two would increase the available space for input hoses and reduced the chances of leakage in future iterations.

The fourth iteration of this design was primarily for purposes of reducing tubing attachment leakage. As recommended by the last iteration, the input passages were reduced by two, improving the available space for attachment of hoses. New 3D printed molds were created as shown in Figure 66 with no difference in dimensions from the third iteration.

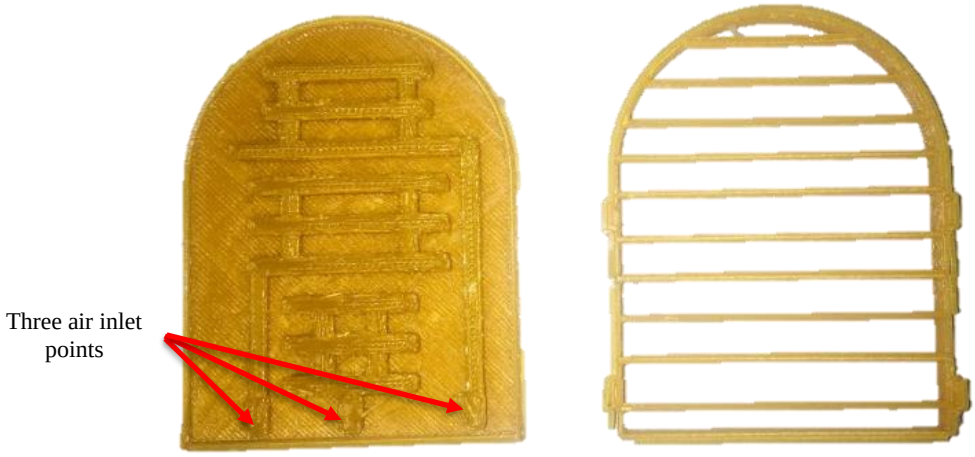

Figure 66 Mold design for the fourth iteration of the prototype.

Silicone molds were made following similar steps in past iterations and the resulting structure are provided in Figure 67. It is evident in this image, by the silicone structure surrounding the inlet passage, that additional support is provided for the inlet tubing.

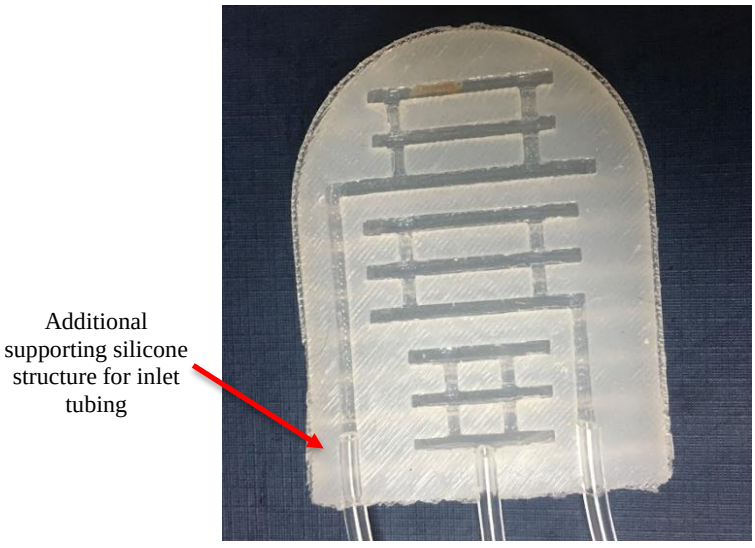

Figure 67 Silicone structure for the fourth iteration of the prototype.

The successful test of this iteration proved that the design changes mitigated the leakage around the air input tubing. An image of the actuator using only three input hoses is provided in Figure 68.

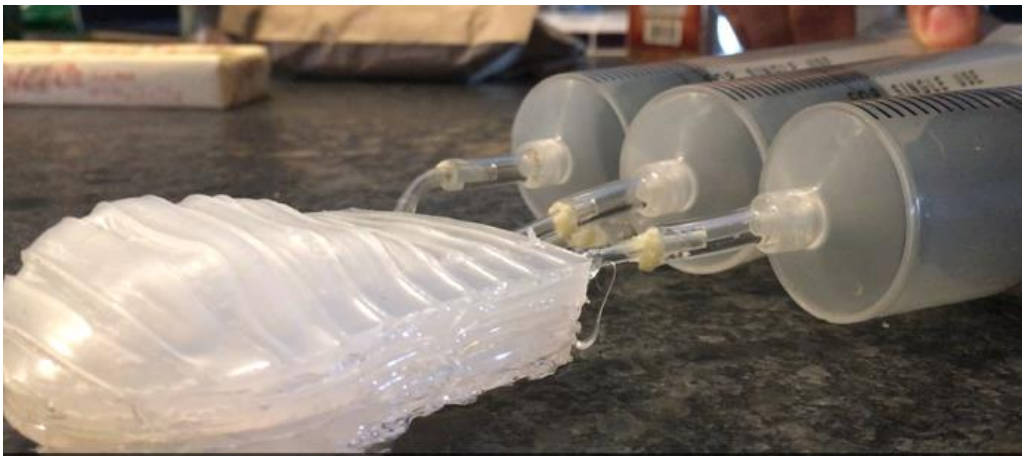

Figure 68 Fourth iteration test actuation with only three input hoses.

The following section applies the learned manufacturing concepts for reshaping the tongue prototype to similar geometries of the human tongue in the following iterations.

Geometry Iterations

At this point of the iteration process, it was determined that a more tongue like shape geometry should be designed for esthetic purposes. Furthermore, it is of importance to ensure that the tongue geometry fits properly inside of the oral cavity in the static or actuating position. A brief literature review was done and concluded large variability in oral cavity measurements. In addition, no available data on the tongue weight was found. This inconsistency in the literature data, made it difficult to determine the correct dimensions of the oral cavity. This information is important for determining the dimensions of the prototype design and the space available for actuation. In turn, it was determined that a better approach would be to take a dental cast using gypsum casting material. This approach provides a more realistic process for post-Glossectomy patients who have variabilities in oral cavity measurements after floor surgical reconstructions. Furthermore, the dimensions of the prototype may change based on the available power source and air chamber designs.

With the aid of Dr. Shaina Darmont and Dr. Ron Holiman, a cast was developed. The process to create the cast began by taking an impression of the oral cavity using soft impression

compound. This negative impression of the gums and teeth, shown in Figure 69 were adjusted with hot wax to resurface any imperfections.

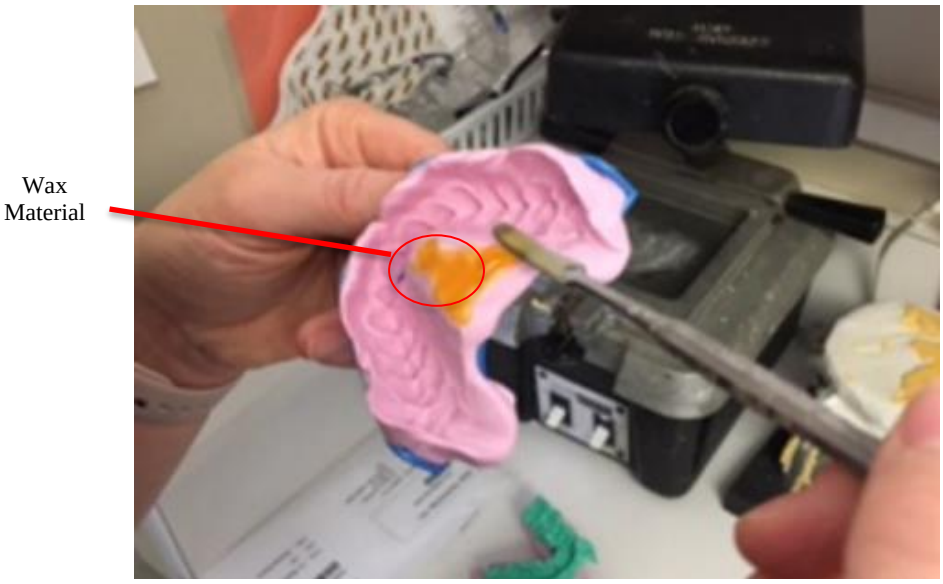

Figure 69 Dental impression wax adjustment.

Once this process was completed, the casting material was mixed as shown in Figure 70 (a) and poured into the finished negative impression. A vibration device shown in Figure 70 (b) was used during this process to ensure air bubbles trapped in the mixture are brought to the surface.

Figure 70 (a) Casting material preparation and (b) Impression pour vibrator use.

At this point, the upper and lower mouth casts were left to cure for approximately one hour on a flat tile surface as shown in Figure 71.

Figure 71 Cast left to cure on flat tile surface.

Once the cast material has cured, the negative impressions casts were removed and trimmed to the approximate anatomical shape. An image of the lower resulting cast is shown Figure 72.

Figure 72 Lower denture resulting cast.

As a final step, the upper and lower casts are mounted on a metal articulator to ensure proper bite positioning. As shown in Figure 73, a bite impression taken from the patient was used to facilitate this process.

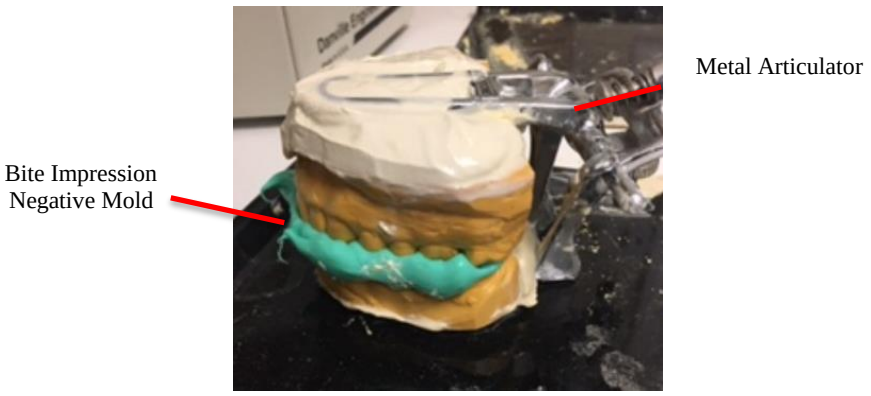

Figure 73 Upper and lower denture articulator mounting.

Once the cast has been mounted, mandibular arc and floor depth can be measured at points shown in Figure 74. These mandibular arc measurements are approximately 1.5 inches in width, 1.6 in length and 0.5 in thickness. These measurements will be used to approximate the design of future iterations of the tongue to determine its manufacturability.

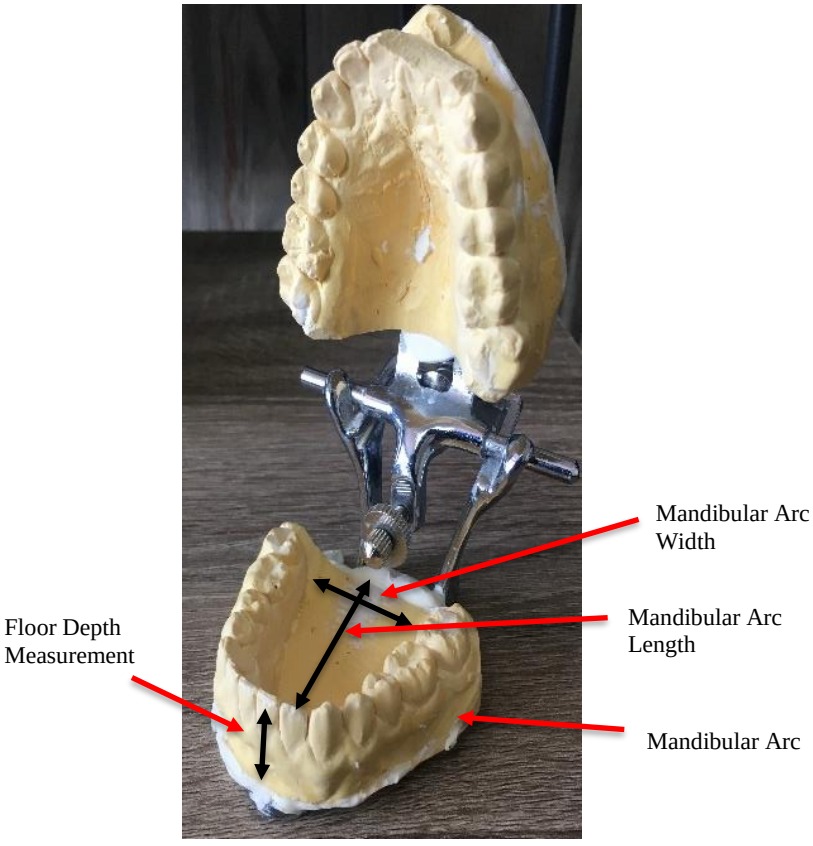

Figure 74 Maxillary and Mandibular Arc measurement.

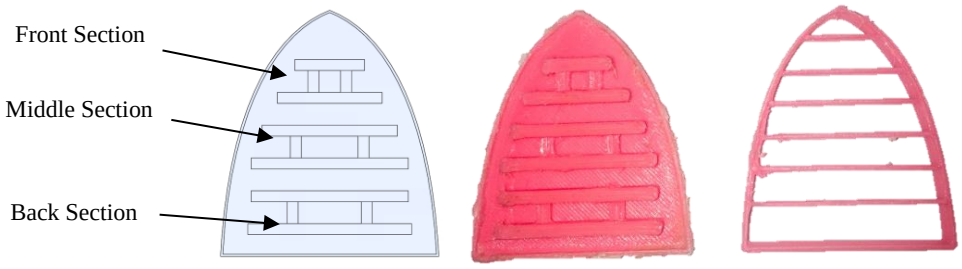

Figure 75 Mold design for the fifth iteration of the prototype.

The measurements attained were used to restructure the last design iteration so that a tongue like shape could be attained. During the CAD design of this iteration, it was determined that the curved perimeter geometry and smaller dimensions would pose space issues for the air passages previously designed on the outer edges of the mold. To mitigate this new obstacle and maintain the dimensions of the air chambers, the air input location was relocated on the underside of the bottom layer. With this solution in mind, the molds were 3D printed as shown in Figure 75. At this scale of iteration, special attention was placed on the quality of the molds to ensure success in molding process. After 3D printing the molds, they were trimmed to ensure tight fit and clean edges. Using a mini digital scale, the silicone 1:1 ratio mixture of Eco-flex 00-30 A and B is poured into the molds until the mixture reaches the top edge. Roughly 0.2 oz of silicone mixture is used when creating the silicone actuators as shown in Figure 76. A mini scale was used in this iteration to provide better accuracy in the silicone mixture. This will facilitate future iteration changes and validation of those changes by controlling aspects as the silicone weight and mixture distribution.

Figure 76 Fourth iteration prototype mixture weight measurement using mini scale.

Similar curing process as previously mentioned were performed on this silicone mixture. An image of the top and bottom layers of the resulting silicone structure is provided in the Figure 77.

Figure 77 Silicone structure for the fifth iteration of the prototype.

The dimensions for this iteration are provided in Table 5. The dimensions comparison for this iteration found the width and height to be relatively similar between CAD model and actuator. Significant length differences were still encountered in this process due to uncontrollable shrinkage of the PLA material.

Table 5 Fifth Iteration Manufacturing Dimensions

Format	**Overall** **L x W x H** **(inches)**	**Air Chamber Row** **L x W x H** **(middle)** **(inches)**	**Air Passage Column L x W x H** **(middle)** **(inches)**	**Assembly Weight** **(ounces)**
CAD Model	2.21 x 1.96 x 0.3	1.44 x 0.1 x 0.1	0.2 x 0.1x 0.05	N/A
PLA Mold	1.69 x 1.5 x 0.25	1.15 x 0.12 x 0.12	0.14 x 0.1 x 0.07	0.1
Silicone Actuator	2.4 x 1.8 x 0.24	1.14 x 0.12 x 0.08	0.14 x 0.09 x 0.06	0.2

Once the silicone structure layers have been removed, both layers are adhered together with additional silicone mixture and pressed firmly with enough force to ensure layers are fully in contact. It is recommended during this process that the top layer remains on top so that any excess silicone mixture does not enter the air passages or chambers. This will prevent any blockage from occurring during the curing process.

Once the adhesion of the two layers has been completed, the final step is to install the input tubing. Since the top layer air chambers require pressurized air input, the bottom layer must be punctured with a pen size pick at the respective locations shown in Figure 78. This provides access to the first air chamber row of each tongue section as shown in Figure 79. Figure 78 also shows an

attempt to use plastic attachment fixtures that were found to be unsuccessful since, once installed, were very difficult to reseal if leakage occurred.

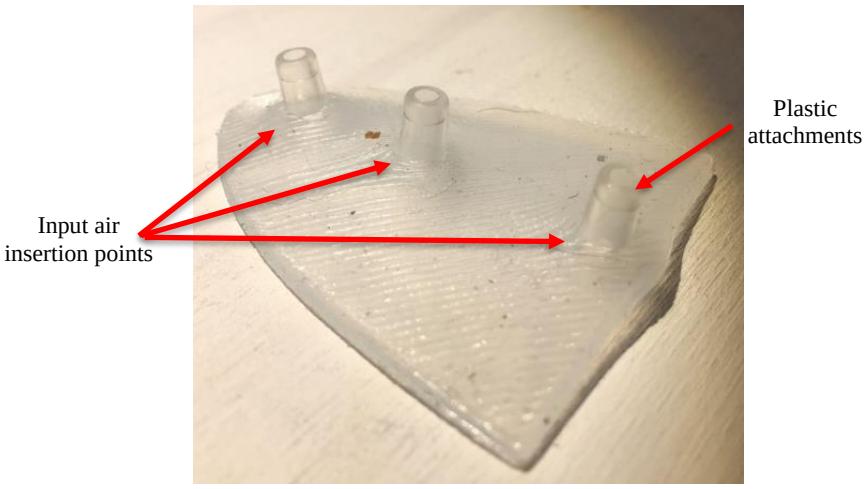

Figure 78 Bottom layer input locations with plastic attachment points.

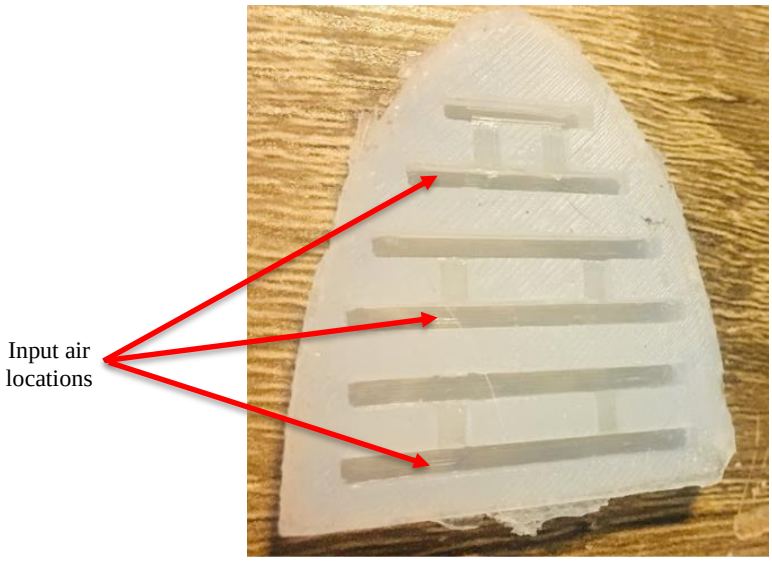

Figure 79 Top Layer location of input air through bottom layer.

The alternative approach for installation was to directly insert the tubing as shown in Figure 80. Its outside circumference was then sealed with high strength silicone RTV adhesive. The RTV was left to cure for 24 hours as with the other iterations.

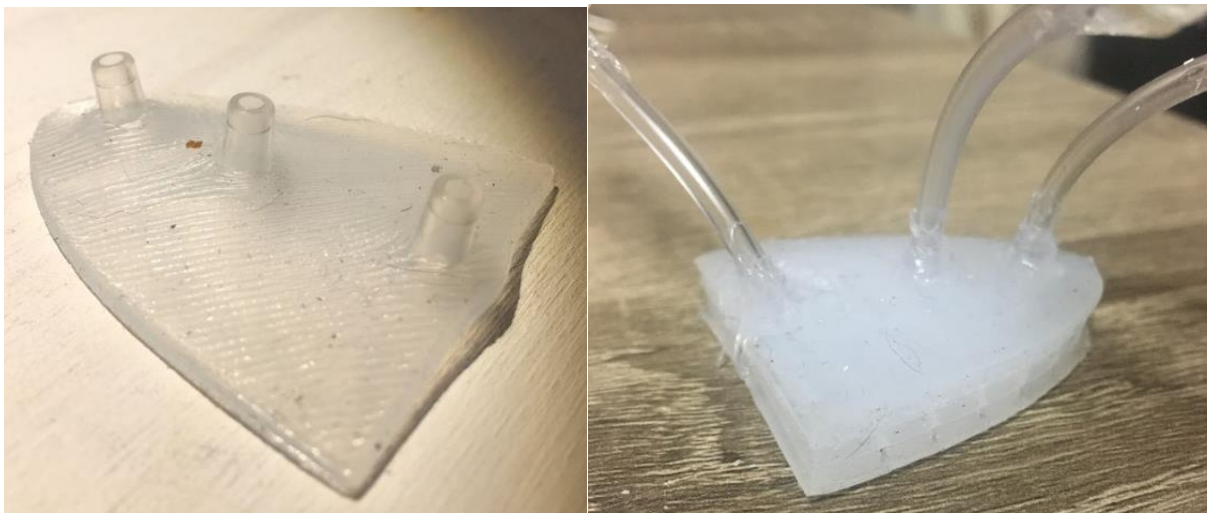

Figure 80 Comparison between (a) before fixture attachment idea and (b) alternative direct attachment of tubing.

The fifth iteration in the geometry iteration process provided insights into design modifications made for adaptability of tongue geometry. As noted in Table 5, the shrinkage of the molds was also experienced in this iteration. In comparison to past iterations, the height of the air passages between air chambers was reduced by 0.02 inches. This done to reduce the possibility of extension at these air passages and allow for the available pressure to be used mostly on the air chambers. Furthermore, the relocation of the input hoses provided improved accessibility to the chambers and reduced the possibility of leakage in the actuator. The final manual testing of this iteration showed wave like motion as in previous iterations.

This chapter has provided information detailing the iterative process and design challenges encountered. The tongue prototype was scaled from its original dimension in inches of 4.6 length, 2.97 width and 0.52 height to final dimensions of 2.4 in length, 1.8 in width and 0.24 in height. The next chapter investigates the development of a prototype testing module. The major components and operational logic are provided. Furthermore, the advantages of the use of this module and learned outcomes are described in detail.

VII. Controls for Testing the Prototype

This chapter provides details about the control system used for testing the scaled tongue prototype iteration. Past testing of prototype iterations used manual syringes to provide pressurized air to the associated air chambers. This method made it difficult for a single researcher to actuate the prototype in a synchronized manner for swallowing motion visualization. The intent of developing this testing module is to not only facilitate the testing process with electrically driven pumps, but also to ensure equal testing parameters are provided for current and future prototype validations.

The controls for the tongue prototype were developed based on the earlier work of Victoria Oguntos found in Soft Robotics Tool Kit website [39]. The major components of the system include, three 6.5 psi mini pneumatic pumps, three two-way solenoid valves and an Arduino Uno microcontroller. An image of these major parts is provided in Figure 81. The test module system is designed to provide on demand pneumatic air input to the silicone actuator for testing of different iterations.

Figure 81 Major parts in testing control system (a) Miniature Air Pumps, (b) Solenoid Valves and (c) Arduino Uno Microcontroller.

The Arduino script logic provided in Figure 82 can be described in the following steps. Once power is supplied to the Arduino by a 9 volt external battery, the air pumps automatically turn on. The microcontroller at this point continuously reads a toggle switch to detect an on or off position. If the switch is physically turned to the on position, the microcontroller automatically provides power to the solenoids. This electrical power develops a magnetic field inside the solenoid that pulls a blocking cylindrical metal piece away from the outlet. This process occurs in a synchronized manner through the use of delay functions which pause the code before moving to the next line of action. This is how the wave like motion is achieved starting with the front section,

then the middle section and finalizing with the back section of the tongue. This synchronized motion remains in an infinite loop until the toggle switch is detected to be in the off position. If this occurs, the system shuts off all power to the solenoids preventing any further actuation of the silicone tongue.

```
/* Arduino Code for Silicone Actuator Controls*/
int buttonState = 0;
void setup() {

/* Set Pins for Arduino Components*/
    pinMode(5, OUTPUT);//Back Section
    pinMode(6, OUTPUT);//Middle Section
    pinMode(7, OUTPUT);//Back Section
    pinMode(4, INPUT);//Switch

}

void loop() {
buttonState = digitalRead(4);//Read Switch to check if On

//Provide power to Solenoids if switch is ON */

if ( buttonState == HIGH) {
digitalWrite(7,HIGH); //Front Section On
delay(200);
digitalWrite(6,HIGH); //Middle Section On
delay(100);
digitalWrite(7,LOW); //Front Section Off
delay(800);
digitalWrite(5,HIGH);//Back Section On
delay (100);
digitalWrite(6,LOW);//Middle Section Off
delay(800);
digitalWrite(5,LOW);//Back Section Off

}
//Remove power to Solenoids if switch is OFF*/
if ( buttonState == LOW) {
digitalWrite(6,LOW);
digitalWrite(5,LOW);
digitalWrite(7,LOW);

}
}
```

Figure 82 Microcontroller Arduino script logic.

To house all the components in the control system, a simple 3D printed structure shown in Figure 83 was created allowing for ease of prototype installation and testing. An image of the final testing module assembly is provided in Figure 84 with the respective major components.

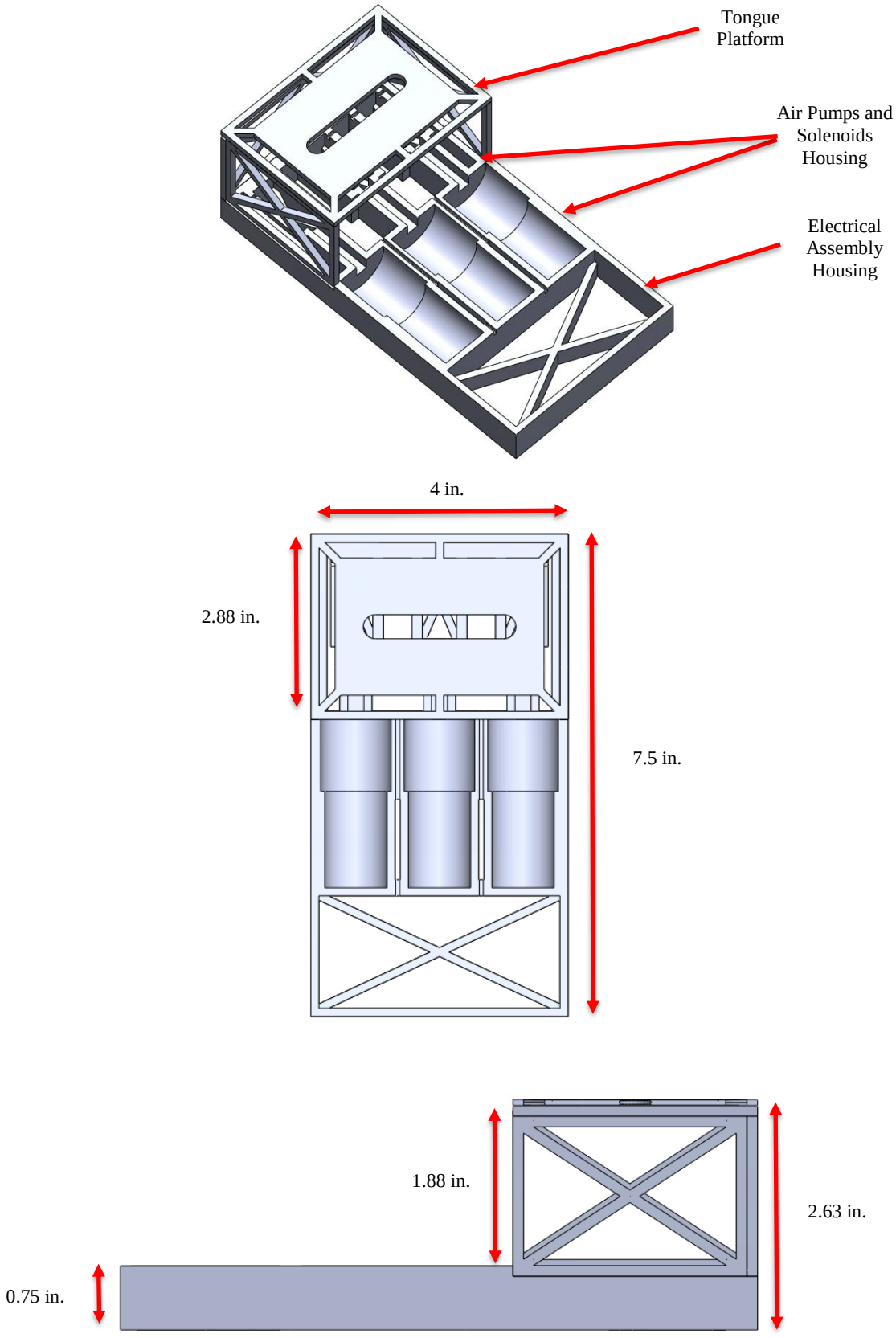

Figure 83 3D model of testing module in (a) isometric view, (b) top view and (c) side view.

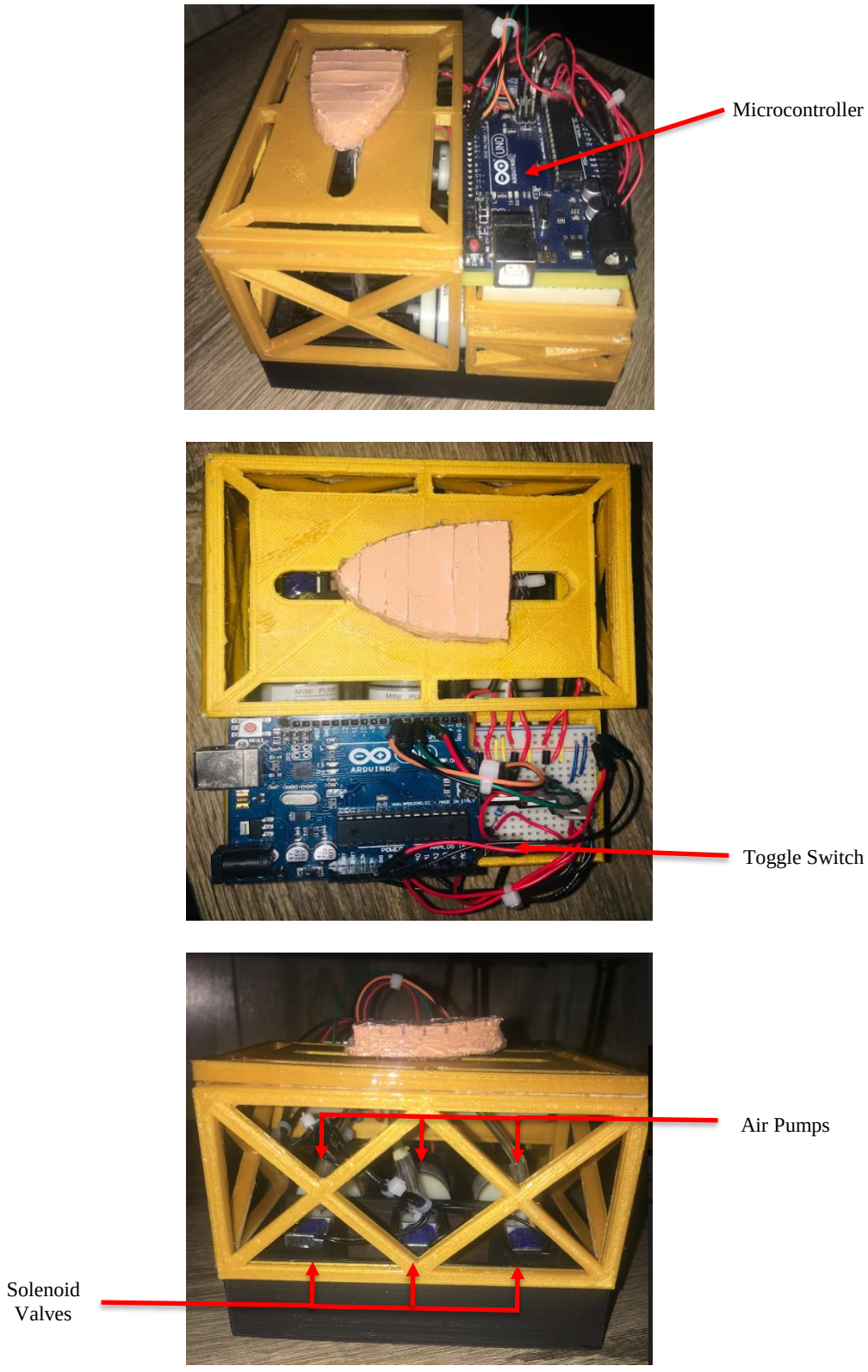

Figure 84 Testing module assembly side view (a), top view (b) and front view (c).

The tongue can be easily mounted by placing the input hoses through the slotted orifice and manually attaching hose ends to the respective solenoids. The Arduino placement allows for the ease in routing of electrical wiring from all pumps and solenoids. The electrical wiring assembly of this system was based on the electrical wiring provided in Figure 85 [39]. This testing module omitted the use of pressure sensors. Future testing module iterations may include the pressure sensor for determining the inlet pressure of each tongue section.

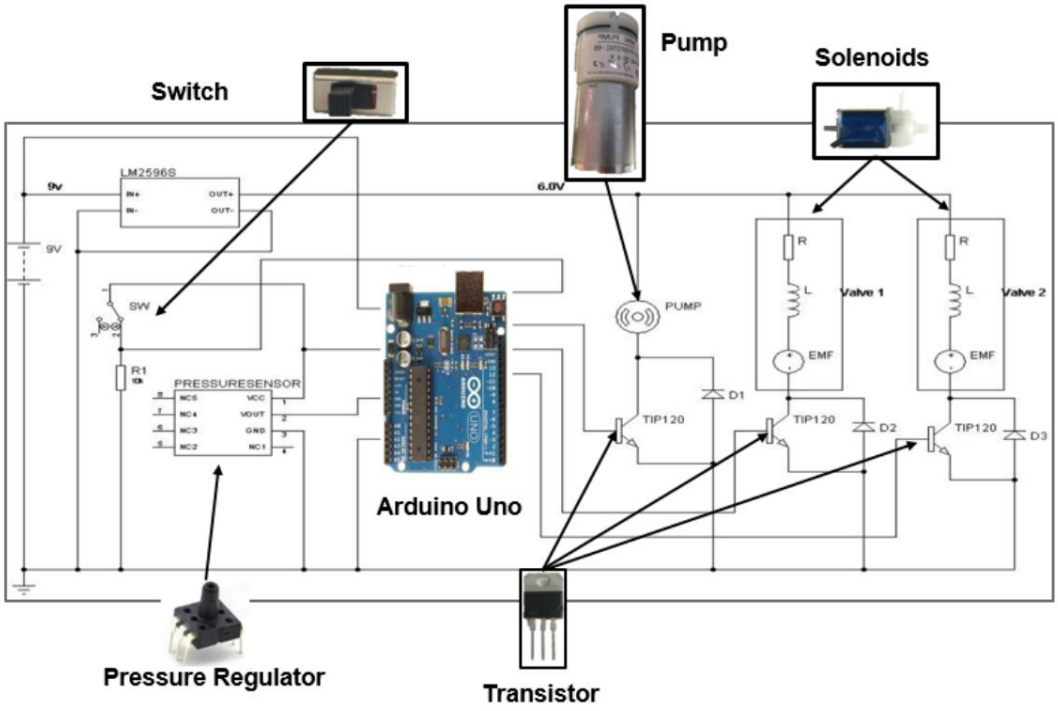

Figure 85 Electrical wiring diagram showing major components used in the electrical assembly [39].

The assembly and test of the module controls was found to be successful through observation of the wave like motion of the tongue prototype. The deflection of the tongue prototype can be seen on the testing module starting with the front deflection (Figure 86), followed with the middle deflection (Figure 87) and ending with the back deflection (Figure 88).

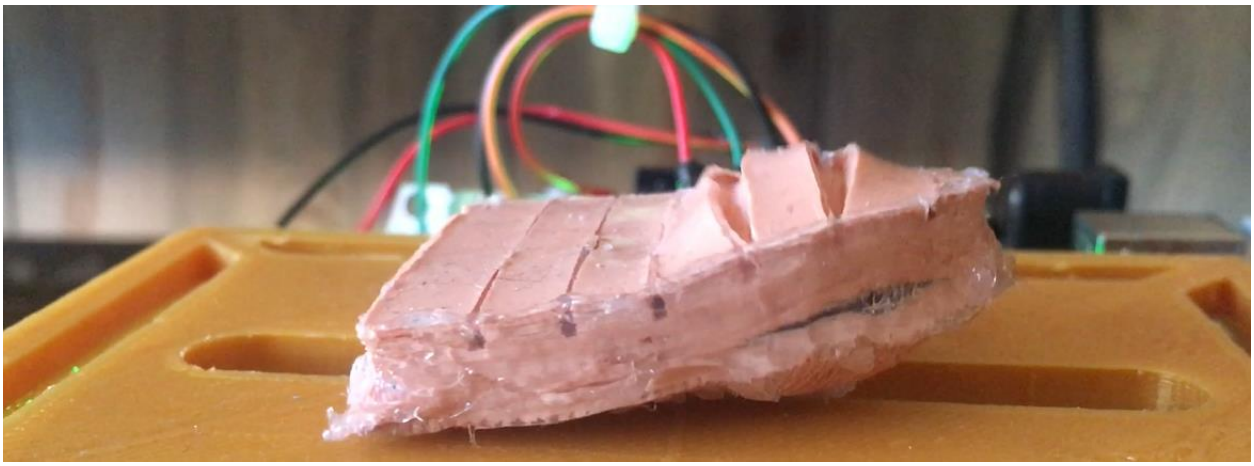

Figure 86 Tongue prototype front section deflection on testing module.

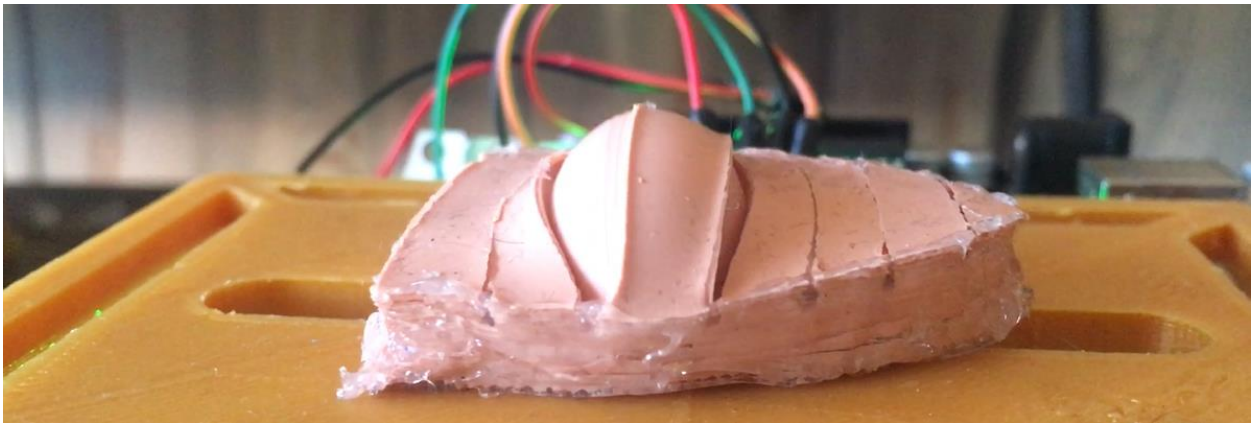

Figure 87 Tongue prototype middle section deflection on testing module.

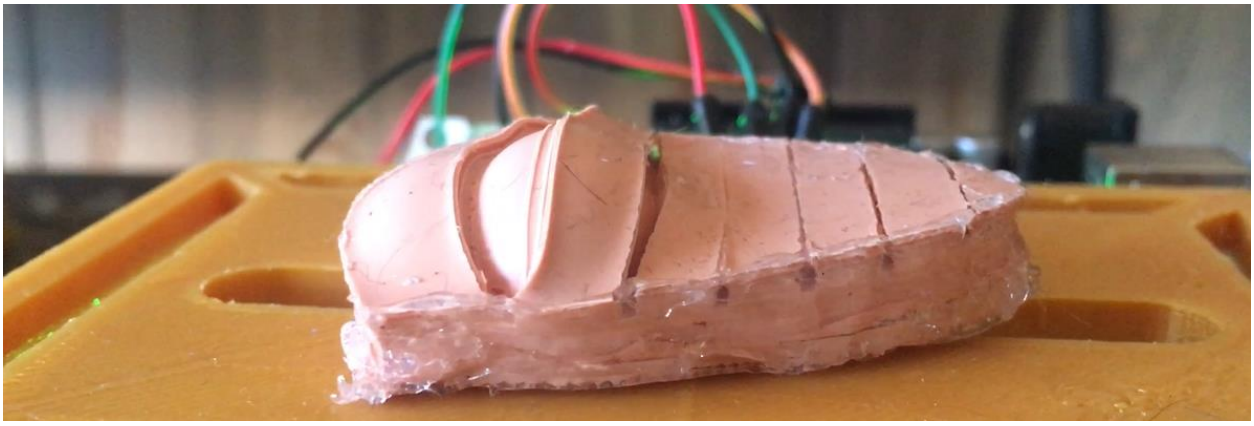

Figure 88 Tongue prototype back section deflection on testing module.

The results of this development will facilitate the validation process of future tongue prototype iterations and provides the necessary components for tongue swallowing actuation. Future work will investigate miniaturizing such system so that it can be integrated into the tongue prosthetic supporting assembly.

The next chapter will provide details of the process taken for validation and analysis of the wave like motion of the prosthetic tongue. Furthermore, the validation process will disclose additional challenges that must be considered to ensure consistent validation practices for future iterations.

VIII. Validation and Discussion

This chapter provides the process taken to setup the Tracking software and the data acquired through this process. Analysis of the gathered position data is provided in detail.

Software and Validation Controls

The first validation step of the latest prototype iteration was focused on the deflection of the respective tongue sections. To begin, an open source tracking software called Tracker [45] was downloaded for analyzing video footage of the prototype in motion. A ruler was then position perpendicular to the prototypes back edge and aligned with the center of the tongue as shown in Figure 89. The purpose of the ruler is to allow the tracking software to use its dimensions as the primary reference for motion analysis. Furthermore, tracking points, represented by black beads, were glued to the top surface of the tongue. Each tracking point was placed approximately between the two air chambers of each section of the tongue. At this point, a video of the tongue in motion was recorded.

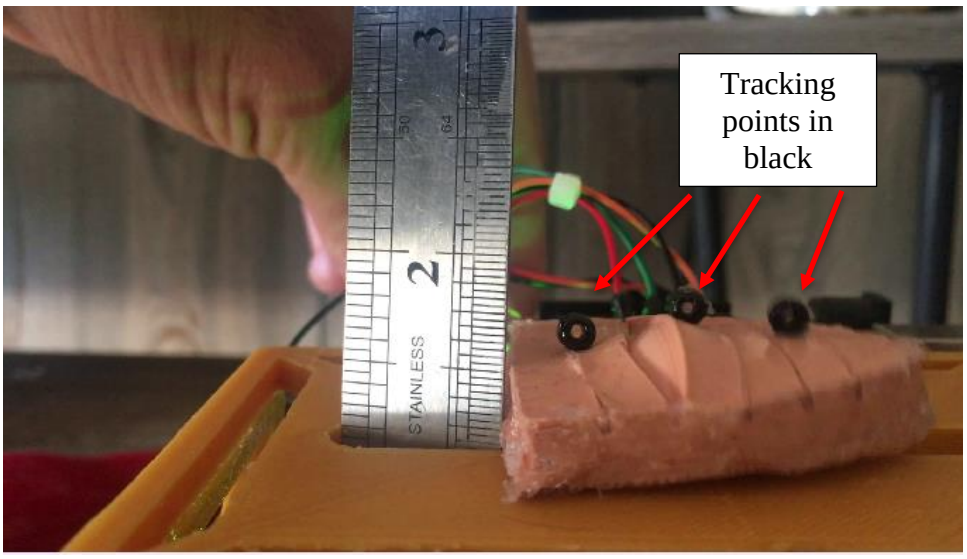

Figure 89 Scale placed behind tongue prototype for reference.

Once a video of the tongue motion was uploaded to the Tracking software, the reference controls were setup in the following process. First, a calibration stick was created to a measurement of 0.5 inches. This measurement is arbitrary, and it is dependent on the units used. Figure 90 provides an image of the location of such reference.

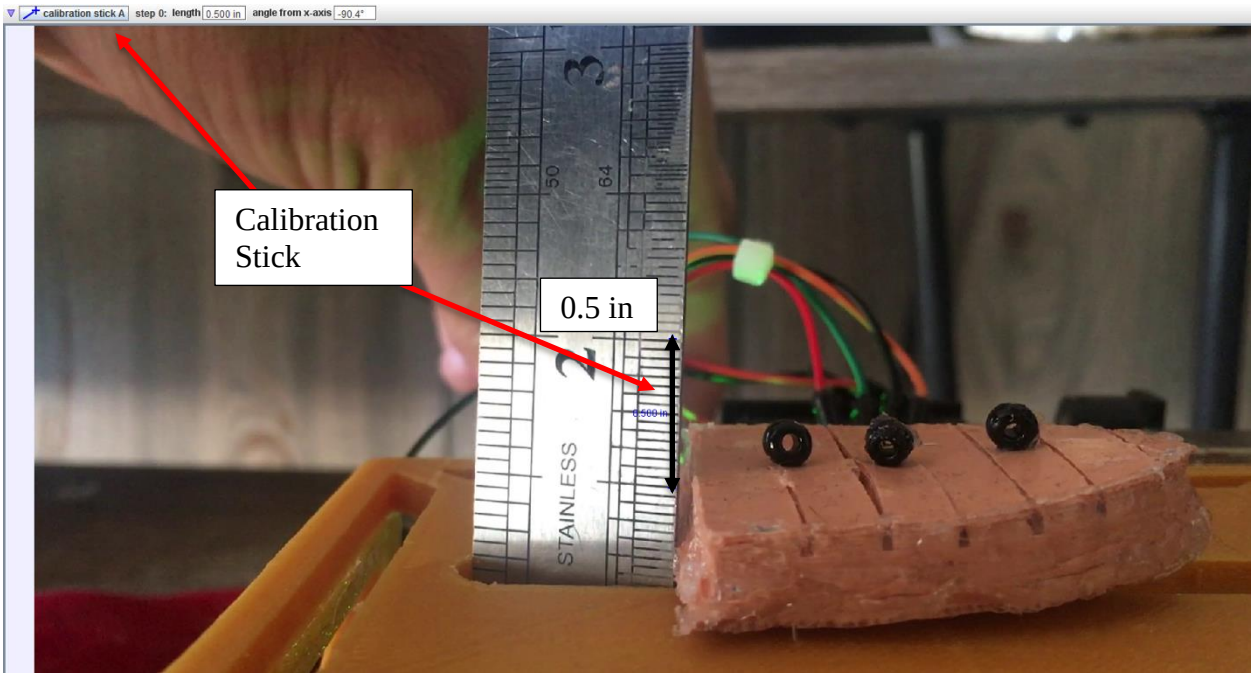

Figure 90 Calibration stick positioning on prototype video.

Then, a coordinate axis was placed on the tongue prototype to provide a reference for deflections in the y direction. Figure 91 provides details of the axis location.

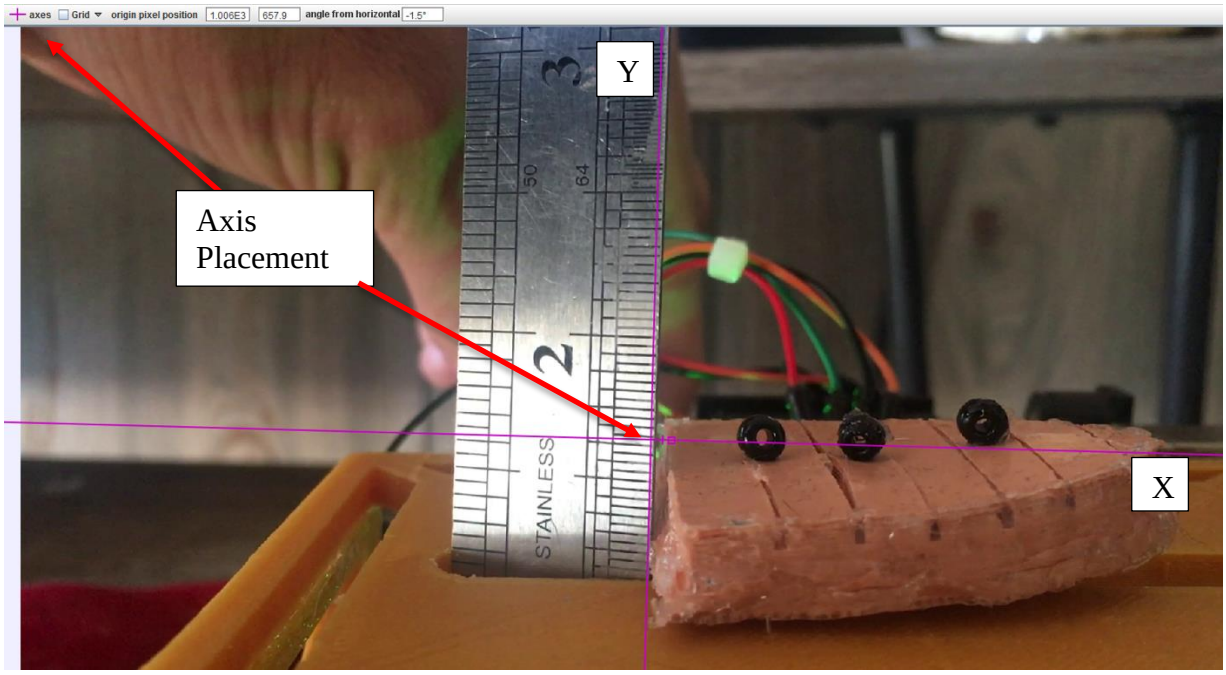

Figure 91 Axis placement on prototype video.

Once the reference setup was completed, each point was automatically tracked with the Tracking software by placing a mass point on each black tracking bead that was glued on the surface of the tongue. A sample of this can be seen in Figure 92.

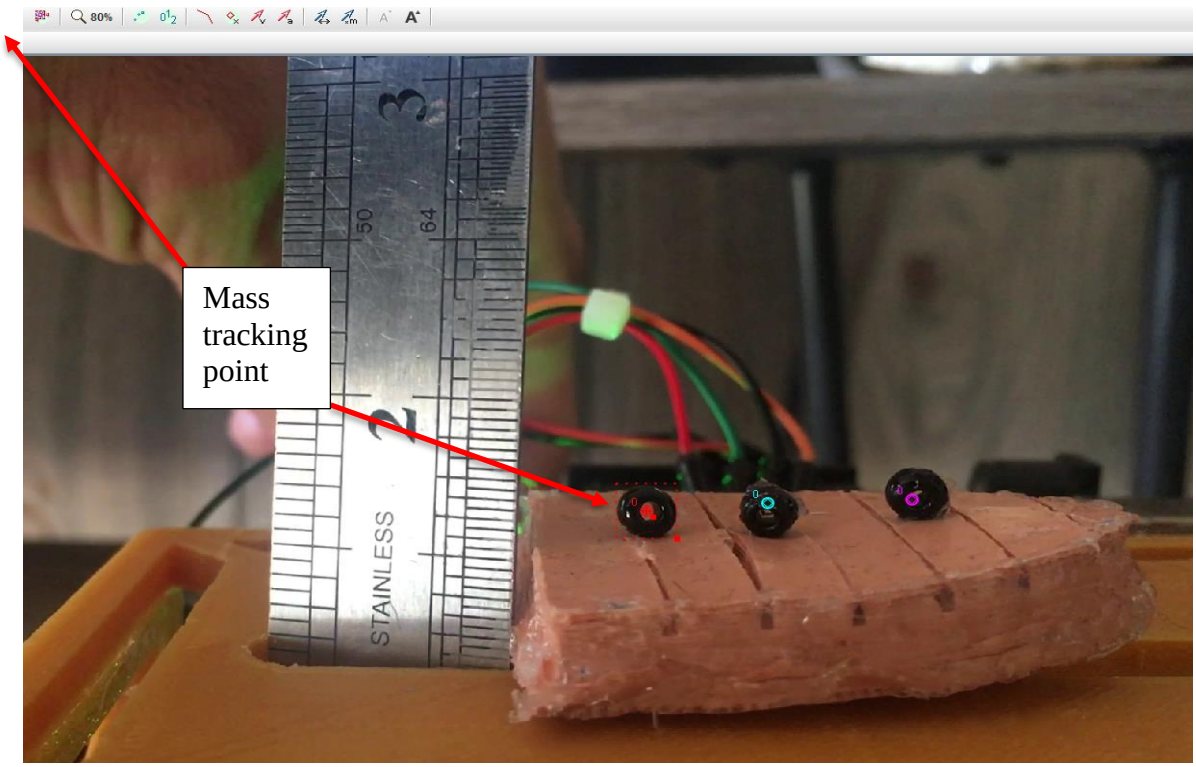

Figure 92 Automatically generated mass tracking point.

Data Acquired

The data acquired through the tracking software includes the position for each section of the tongue in respect to the y axis.

Theoretical Position Estimation

The theoretical data was calculated using fundamental bending deflection theory for a simply supported beam. This theory was chosen because it resembles the static support set up of the tongue prototype silicone structure. Furthermore, it allows for simplification of the silicone structure for analysis. The theoretical equation used for determining the bending deflection (δ_{max}) in the y direction of each chamber is provided in Equation 3. It is composed of the length of the chamber (L), the load distribution (P), the Modulus of Elasticity (E) and the Moment of Inertia (I) (Equation 4). Each section of the tongue is composed of three rectangular beam sections under

pressure, two for the air chambers and two for the air passage chamber. This maximum deflection is assumed to be located at half the length of the beam member. The distributed force per length of each chamber is assumed to be uniform at 0.65 psi. The modulus of elasticity for silicone was referenced to be approximately 18.13 (psi) [43]. Typical Moment of Inertia values for this prototype ranged from 2.8 to 6.6 E-5. No lateral deflection of the silicone actuator is considered in this simplified theoretical model.

$$\delta_{max} = \frac{5PL^4}{384EI} \tag{3}$$

$$I = \frac{wh^4}{12} \tag{4}$$

Figure 93, Figure 94 and Figure 95 provide a detail view of the theory and representation of these equations. Figure 95 is the final representation of the rectangular silicone beam sections shown above the air chambers in Figure 94. The height of this beam is measured in the Y axis and the length is measured in the X axis.

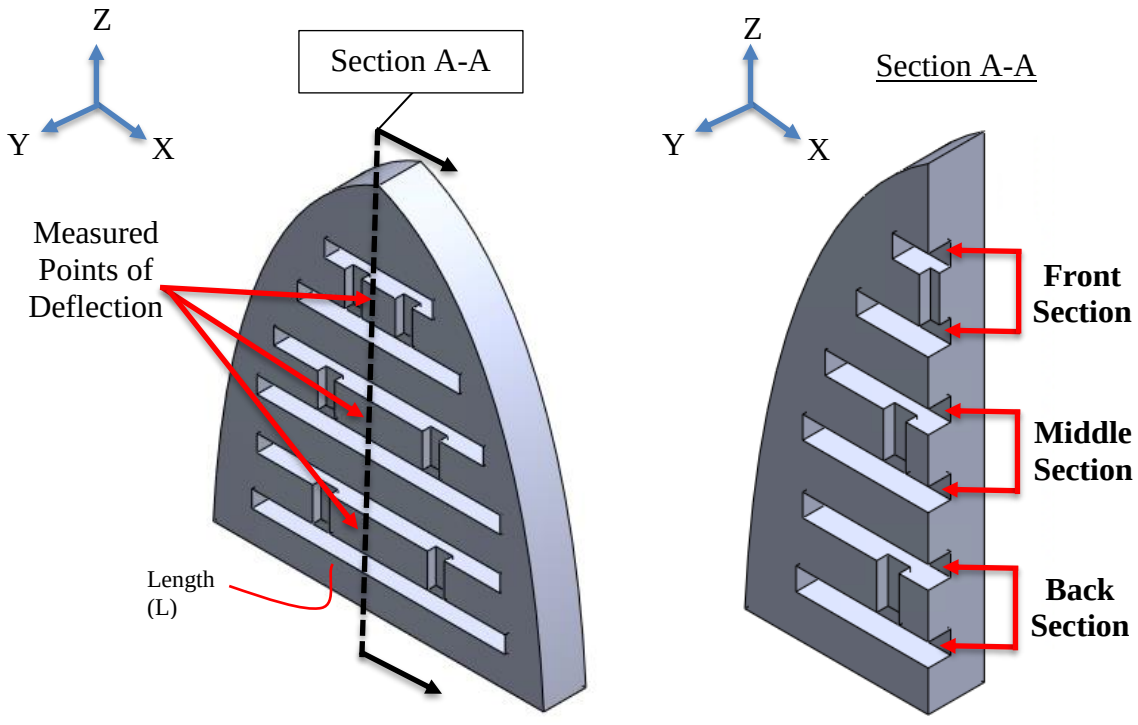

Figure 93 Silicone tongue (a) assembly and (b) section A-A cut view.

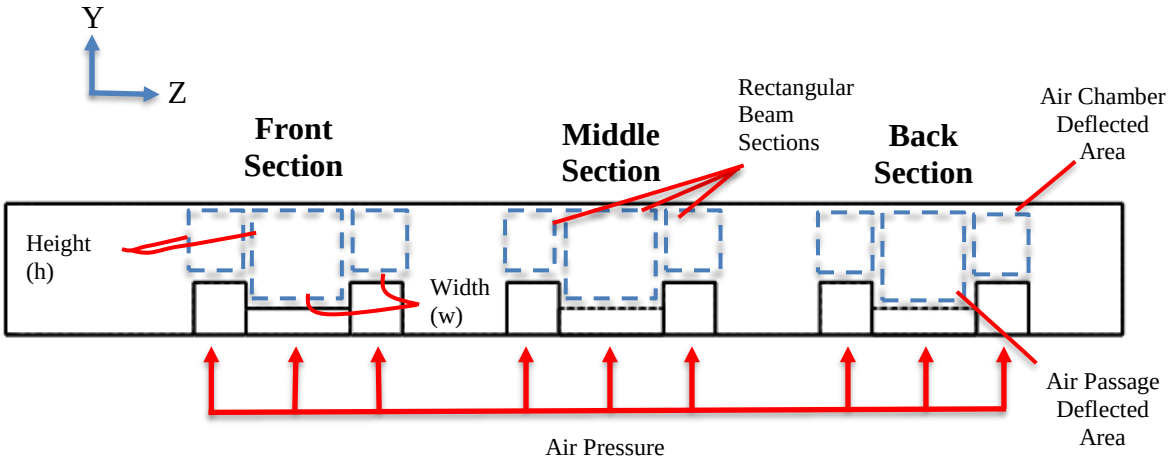

Figure 94 Section A-A cut front view displaying rectangular beam sections being analyzed for bending deflection.

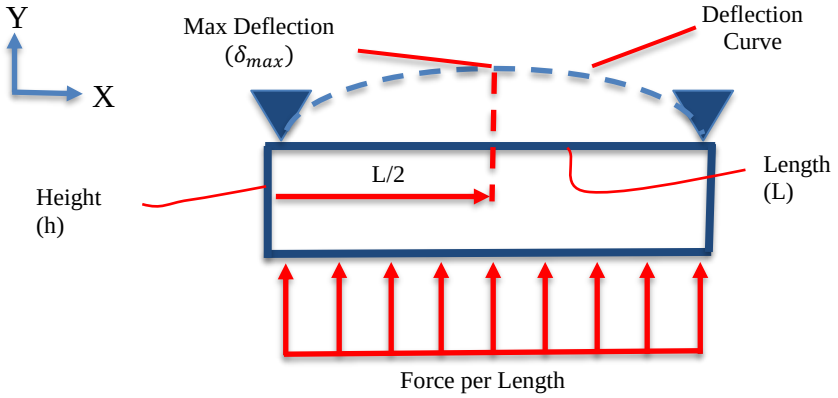

Figure 95 Theoretical rectangular beam deflection model under uniform force per length.

Position Data Comparisons

The following figures provide the position and experimental data acquired during the latest prototype iteration analysis. These figures include, Front Section Deflection, Middle Section Deflection and Back Section Deflection.

The max deflection of the front section (Figure 96) of the tongue was measured to be approximately 0.417 inches. This differs from the T2 position of 0.413 inches with a standard deviation of 0.17 inches found in the literature review. The difference in time from no deflection to point of highest deflection is approximately 0.4 seconds.

The position of the middle section of the tongue (Figure 96) was measured to be approximately 0.454 inches. This differs from the T3 position of 0.598 inches with a standard

deviation of 0.114 inches found in the literature review. The difference in time from no deflection to point of highest deflection is approximately 1.02 seconds.

The position of the back section of the tongue (Figure 96) was measured at approximately 0.242 inches. This differs from the T4 position of 0.751 inches with a standard deviation of 0.093 inches found in the literature review. The difference in time from no deflection to point of highest deflection is approximately 0.55 seconds.

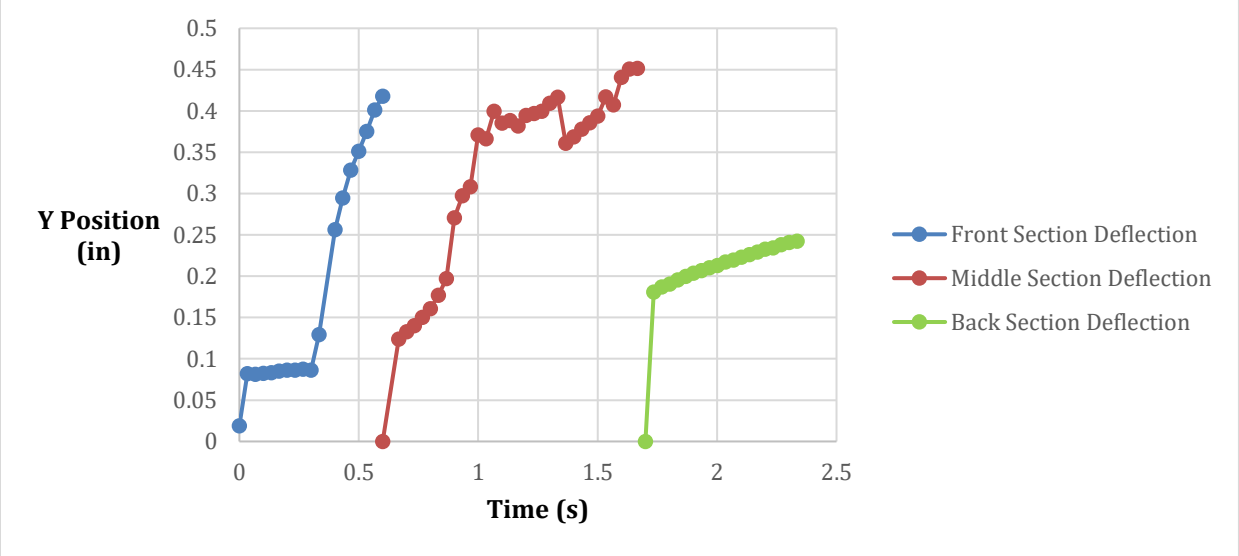

Figure 96 Deflection of the front, middle and back sections of the tongue prototype during testing.

Discussion and Analysis of Data

The overall data results and comparisons for the first prototype test can be summarized in Figure 97 showing all three points (T2, T3 and T4) compared against experimental data. It is clear through this chart that the deflection and time of deflection of the prototype does not match with literature review data. Furthermore, the theorized deflection calculations are substantially higher for all sections when compared with the experimental data. The summary of deflections can be seen in Table 6.

Table 6 Comparisons of deflections between literature review, experimental and theoretical data.

Total Deflection Comparison			
Data Sections	**Front (in)**	**Middle (in)**	**Back (in)**
Literature Review Data	0.41	0.6	0.75
Experimental Data	0.42	0.45	0.16
Theoretical Data	16.9	110	168

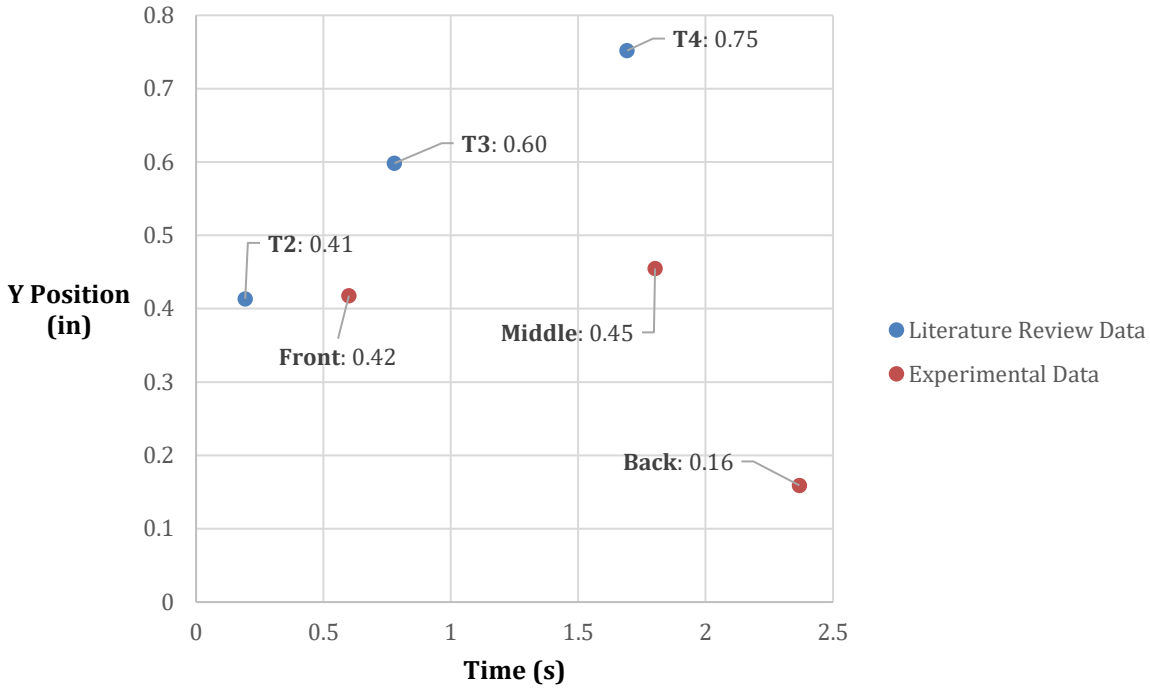

Figure 97 Summary of Literature versus Experimental data points.

This difference in deflection is theorized to be associated with several factors. First, during the operation of the tongue prototype, lateral deflection of the air chamber walls was noted which could have a restrictive effect on the deflection in the y axis direction. Secondly, since the internal pressures of the air chambers were not quantified in this first iteration test, the rated value of the air pumps of 6.5 psi was used to determine the force per length of the chamber. The pressure inside the chamber is theorized to be substantially lower which would reduce the overall theorized deflection. Thirdly, the values gathered in the literature review differ between male and female genders and are based on a small number of subjects. Since the dimensions of the prototype were based on one male subject, a true comparison cannot be achieved with the literature data. Fourthly, the silicone material modulus of elasticity for Eco-flex 00-30 of 18.13 psi may be affected by environmental, cycling and manufacturing factors. This could have a direct impact on the resistant force of the material in the deformation state. Furthermore, this modulus of elasticity showed variabilities between 8.7 to 18.13 psi in different scholarly articles. This makes the material properties difficult to estimate. Finally, the simple theoretical equations (3) and (4) used, do not consider the nonlinear stress and strain properties of silicone materials and other contributing factors. This puts into question the reliability of the calculated values. Future prototype testing

processes will focus on controlling and quantifying these factors to provide reliable theorized values for comparison.

Software Observations

The tracking software used for this test experienced some difficulties in consistently recording the position of the tracking point at set intervals. It is theorized that this may be due to the tracker point color similarities with the video background. This can be seen in the data gathered at each section by the inconsistent intervals of data provided. This is important to correct in future analysis to prove that the maximum deflection data point collected is indeed the highest deflection achieved by the section. A better tracking point and background contrast will be implemented in future prototype testing processes to correct this issue.

Hardware Observations

The first observation on the hardware relates to the point trajectory trend of each of the sections. It is theorized that the differences and inconsistencies in the trajectory slopes of each section may be due to the prototype upper surface ballooning near the tracking point. This theory is further reinforced by inconsistencies of the trajectory slope when comparing front and back sections with middle section data trajectories. This issue will be resolved in future iterations by controlling prototype manufacturing processes and top layer surface silicone thickness.

A second observation relates to the hose attachment set up shown in Figure 98. Due to the rigidity of the hoses used for air input and the lack of slack provided, the prototype experiences a downward force on the bottom layer. This limits the ability for the upper layer to extend and develop a bending deflection motion. Future prototype iterations will focus on providing more flexible means of input hose attachments.

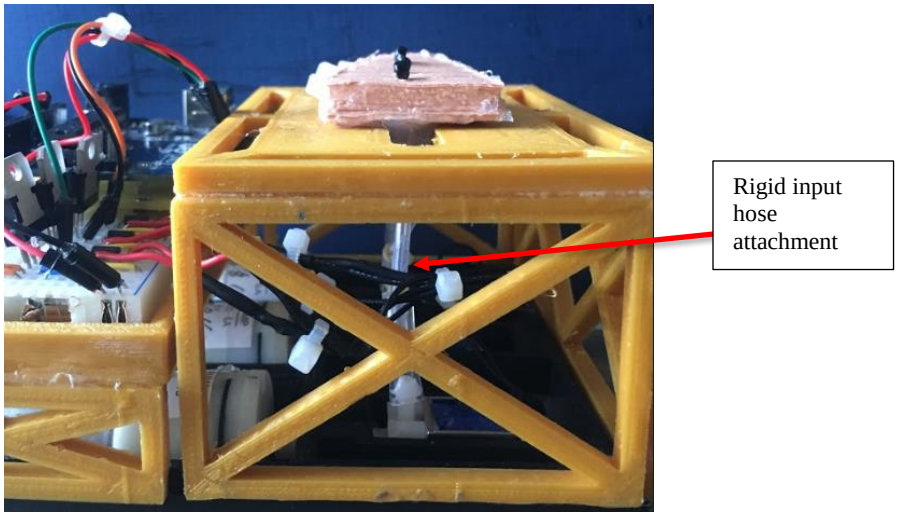

Figure 98 Hose attachment setup.

Finally, the lateral expansion of the tongue back section shown in Figure 99, is theorized to be limiting the axial stress developed on the air chamber walls. Furthermore, the unevenness of this lateral expansions discloses some internal issues with air pressure distribution that are associated with improper bonding of air chamber walls in the top layer. These manufacturing issues will be address in future iterations by embedding rigid mesh like materials in hope of reducing the elastic properties of the lateral walls and ensuring a consistent bond between top and bottom layers.

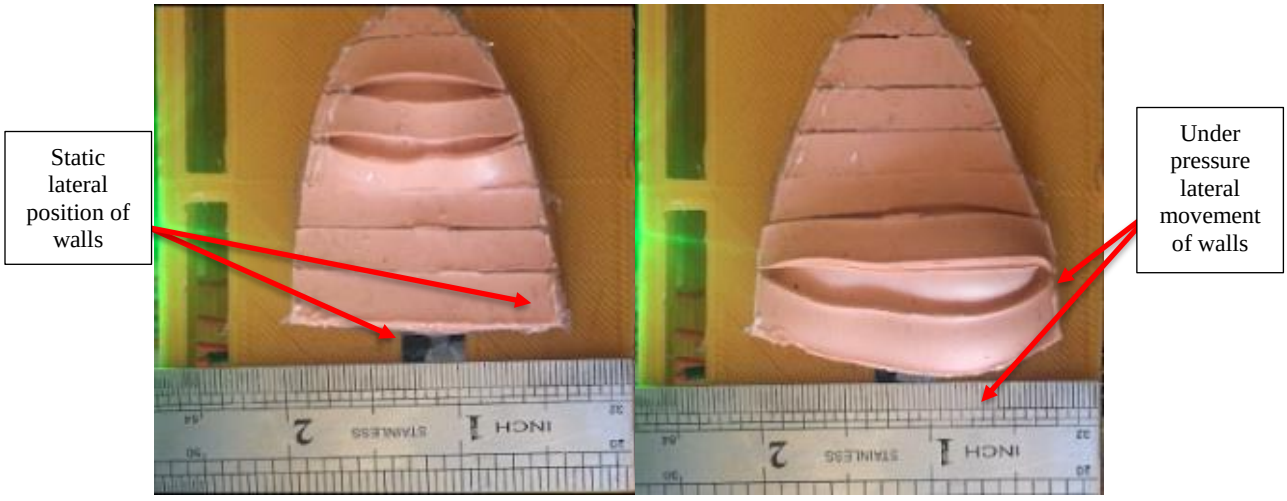

Figure 99 Lateral deflection of tongue.

The next chapter will discuss prototype development conclusion and future work related to the design objectives of the final tongue prosthesis.

IX. Conclusions and Future Work

This chapter provides details on the conclusions and future work of this research. The future work section includes topics as prototype bolus test, mold manufacture medium, tongue surface geometry and simulation software considerations. A summary of the advancements of this research are provided in detail.

Conclusion

The work performed in this research has advanced the development of tongue prosthetics in many ways. This research has provided extensive supporting literature on the importance of developing tongue prosthetics for Total Glossectomy patients. It has also collected important anatomical and kinematic scholarly articles that facilitate the understanding of tongue motion for prosthetic design. The idea of implementing PneuNet systems has been proven through this research as being a viable solution for tongue prosthetics. A tongue prosthetic using silicone PneuNet design theory has been created and tested successfully for wave like motion. Motion data of this prototype and analysis has been provided to facilitate future design iterations. Manufacturing processes challenges for PneuNets systems were identified and solutions provided through this research. Future work recommendations and further prototype areas of research have been identified in detail.

Challenges

This research has disclosed challenges in the development of tongue prostheses. First, the lack of data available for developing PneuNet structures increased the issues encountered through the investigation and application of manufacturing process. These issues relate largely on air leakage resulting from factors as quality of silicone molds, layer adhesion, miniaturization and input hose location and attachment. Secondly, the lack of available data on swallowing and tongue parameters of the tongue, make it difficult to conclude on definitive tongue dimensions. This lack of data makes it difficult to develop exact tongue motions that could facilitate the transfer of bolus to the oropharyngeal section of the mouth. Finally, a large challenge that has been identified through this research is the necessary power accessories for actuation. The items provided in the prototype testing section, will have to be miniaturized and implemented in the supporting structure of the prosthetic. The technology was not available at the current time of this research to allow for the implementation into the prototype supporting structure and in the oral cavity.

Future Work

The future work of this research seeks to investigate the additional areas that will contribute to the efforts in developing a complete tongue prosthesis. These areas include prototype bolus test, mold manufacturing medium, tongue surface geometry and simulation.

Prototype Bolus and Pressure Test

The prototype cast will be instrumental in testing the bolus movement of the prototype tongue. The maxillary arc in the cast can be used to test if a bolus like structure can be moved towards the back of the oral cavity. Figure 100 (a.) provides a view of the prototype inside of the oral cavity. Its deflection starts with the front section (b.), followed by the middle section (c.) and ending with the back section (d.). In addition, this cast will be vital in providing the surrounding structure for testing the pressure of the prosthetic on the upper palate. By implementing pressure sensors on the palate of the cast, data can be retrieved and analyzed based on anatomical scales. Furthermore, Equation 4 will be fundamental in determining the torque of the actuator based on the attachment point. This will contribute in the analysis of tongue prototype pressure against the hard palate.

Mold Manufacture Medium

The use of FFF for developing the silicone molds was found to be successful to the extent of this research. Future iterations would benefit from more precise mold mediums that can reduce surface imperfections that are theorized to contribute to the air leakage between layers. These other systems may include injection molding, milling, laser cutting and higher quality 3D printing systems. It is recommended for future mold iterations to consider designs that facilitate the removal of mold parts without damage to silicone structures

Tongue Surface Geometry

The tongue surface has a very specific geometry that contributes to the control of the bolus during the swallowing process. Future iterations of the prototype surface should focus on developing bolus contact surface with similar human like functions. A specific area to start with is understanding the geometry of human tongue structures known as filiform papillae. Composed of “fine, small, cone-shaped” geometry as shown in Figure 101 (reproduced as is from [42]), filiform papillae provide the necessary area to develop enough friction against the bolus [40,41].

Understanding the geometry and the types of manufacturing process in developing such micro scale surface textures, will aid in the development efforts of creating an advanced tongue prosthetic.

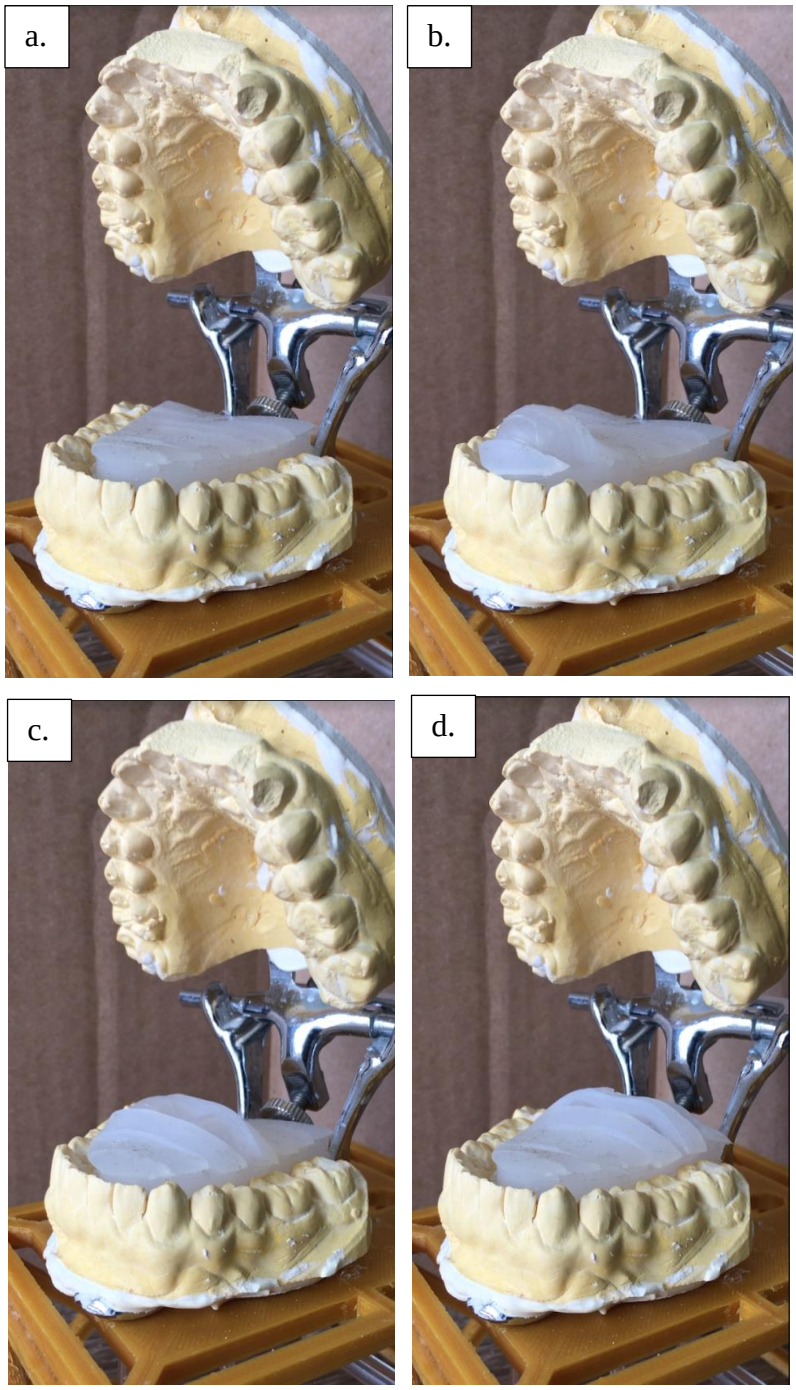

Figure 100 Tongue Prototype inside cast cavity in a). static position, b) front section deflection, c) middle section deflection, d) back section deflection

.

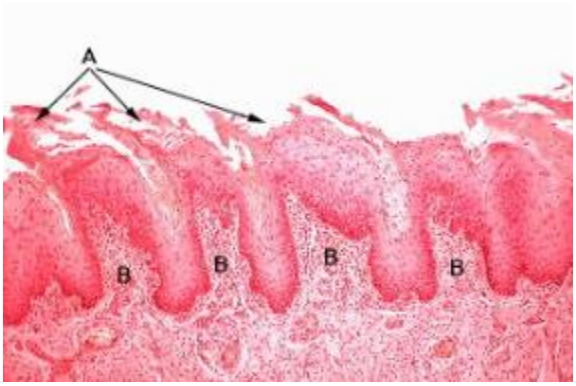

Figure 101 Filiform Papillae shown at A locations (reproduced as is from [42]).

Simulation

Finally, work on the area of simulation software will be beneficial in the development of future iterations. As seen in the Figure 102, software systems as Abaqus, can be used to replicate PneuNet like structures. The theoretical changes in parameters can be used to not only increase understanding of PneuNet motion but also for visualizing the deflection expected for such changes in air chamber parameters. Once replicated, the simulation can be instrumental in the validation process of the prototype.

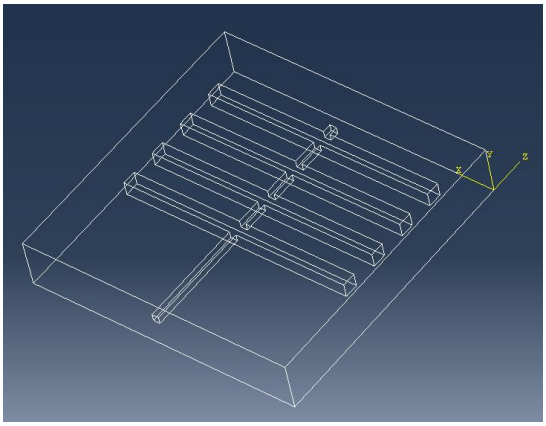

Figure 102 Abaqus PneuNet basic simulation structure.

X. References

[1] Burck, J.M., Bigelow, J.D. and Harshbarger, S.D., 2011. Revolutionizing prosthetics: Systems engineering challenges and opportunities. *Johns Hopkins APL Technical Digest*, *30*(3), pp.186-197.

[2] Florida man becomes first person to live with advanced mind-controlled robotic arm. (2018, February 03). Retrieved from https://futurism.com/mind-controlled-robotic-arm-johnny-matheny/

[3] Organ care system by transmedics by Transmedics Medical Expo. Retrieved October 25, 2018, from http://trends.medicalexpo.com/project-45668.html

[4] Ballingall, Alex. "Heart in a box: will a new technology extend the six-hour transportation time limit for heart transplants?" *Maclean's*, 21 Nov. 2011, p. 68+. *Academic OneFile*, http://link.galegroup.com/apps/doc/A273420100/AONE?u=mlin_c_worpoly&sid=AONE&xid=7e5a70f2. Accessed 25 Oct. 2018.

[5] Siegel, R. L., Miller, K. D. and Jemal, A. (2018), Cancer statistics, 2018. CA: A Cancer Journal for Clinicians, 68: 7-30. doi:10.3322/caac.21442

[6] Cancer Stat Facts: Oral Cavity and Pharynx Cancer. Retrieved October 17, 2018, from https://seer.cancer.gov/statfacts/html/oralcav.html

[7] Gooi, Zhen et al. (2015) Temporal trends in head and neck cancer surgery reconstruction. *Head & Neck*. [Online] 37 (10), 1509-1517.

[8] Hamamoto, Yusuke et al., The Double-Tongue Method: A new reconstruction technique for oral floor reconstruction after total glossectomy. Journal of Plastic, Reconstructive & Aesthetic Surgery, 68(11), pp.1624–6.

[9] Selber, J. C., & Robinson, J. (2014). The Manta Ray Flap. *Plastic and Reconstructive Surgery*, *134*(2). http://doi.org/10.1097/prs.0000000000000315

[10] Longo, B., Pagnoni, M., Ferri, G., Morello, R., & Santanelli, F. (2013). The Mushroom-Shaped Anterolateral Thigh Perforator Flap for Subtotal Tongue Reconstruction. *Plastic and Reconstructive Surgery*, *132*(3), 656–665. http://doi.org/10.1097/prs.0b013e31829acf84

[11] Carvalho, Viviane de & Sennes, Luiz Ubirajara, 2016. Speech and Swallowing Data in Individual Patients Who Underwent Glossectomy after Prosthetic Rehabilitation. International Journal of Dentistry, 2016(2016), p.11.

[12] Alhajj, Mohammed Nasser, Ismail, Ibrahim A. & Khalifa, Nadia, Maxillary obturator prosthesis for a hemimaxillectomy patient: A clinical case report. *The Saudi Journal for Dental Research*, 7(2), pp.153–159.
[13] Sabouri, Amir A. et al., Prosthodontic Rehabilitation for Total Glossectomy with a Magnetic Detachable Mandibular Tongue Prosthesis: A Clinical Report. (Clinical report). *Journal of Prosthodontics*, 21(5), pp.404–7.
[14] Penn, Mark et al., Implant-retained feeding aid prosthesis for a patient following total glossectomy and laryngectomy: A clinical report. (Author abstract) (Clinical report). *The Journal of Prosthetic Dentistry*, 97(5), pp.261–5.
[15] Pravin Bhirangi et al. (n.d.) Technical Considerations in Rehabilitation of an Edentulous Total Glossectomy Patient. *International Journal of Dentistry*. [Online] 2012 (2012), 125036. [online]. Available from: https://doaj.org/article/183fa34888fa46b2a06efe2bbac706da.
[16] Haisfield-Wolfe, Mary Ellen et al., Prevalence and correlates of depression among patients with head and neck cancer: a systematic review of implications for research. (Online Exclusive Article) (Report). *Oncology Nursing Forum*, 36(3), pp. E107–25.
[17] Image Gallery: Muscular Tongue. Retrieved October 26, 2018, from http://keywordsuggest.org/gallery/1004609.html
[18] OpenStax, L. L. (n.d.). Anatomy and Physiology I. Retrieved October 5, 2018, from https://courses.lumenlearning.com/ap1/chapter/axial-muscles-of-the-head-neck-and-back/
[19] Bernal, M. (2012, February 7). Retrieved October 15, 2018, from https://www.youtube.com/watch?v=Yg_kAqBlp9Y
[20] Tasko, Stephen M., Kent, Raymond D. & Westbury, John R., Variability in Tongue Movement Kinematics During Normal Liquid Swallowing. (Author abstract). *Dysphagia*, 17(2), pp.126–138.
[21] Ono, Takahiro et al. (n.d.) Pattern of Tongue Pressure on Hard Palate During Swallowing. *Dysphagia*. [Online] 19 (4), 259–264.
[22] Kawamura, T., Tandai, T. & Takanobu, H., 2005. Mechanism and control of tongue robot. In *Intelligent Robots and Systems, 2005. (IROS 2005). 2005 IEEE/RSJ International Conference on*. USA: IEEE, pp. 1041–1046.

[23] Lu, Xuanming, Xu, Weiliang & Li, Xiaoning, A Soft Robotic Tongue—Mechatronic Design and Surface Reconstruction. Mechatronics, IEEE/ASME Transactions on, 22(5), pp.2102–2110.
[24] Yamakita, T., Obokawa, Y., Eguchi, K., Ishii, H., & Taknishi, A. Retrieved September 21, 2018, from http://www.takanishi.mech.waseda.ac.jp/top/research/index.htm.
[25] Fukui, K et al. (n.d.) Production of Various Vocal Cord Vibrations Using a Mechanical Model for an Anthropomorphic Talking Robot. *Advanced Robotics*. [Online] 26 (1-2), 105–120. [online]. Available from: http://search.proquest.com/docview/1022885603/.

[26] Fukui, K et al. (2009) 'Three dimensional tongue with liquid sealing mechanism for improving resonance on an anthropomorphic talking robot', in *2009 IEEE/RSJ International Conference on Intelligent Robots and Systems*. [Online]. October 2009 IEEE. pp. 5456–5462.

[27] Michel, C., Velasco, C., Salgado-Montejo, A., & Spence, C. (n.d.). The Butcher's Tongue Illusion. *Perception*, *43*(8), 818–824. doi:10.1068/p7733

[28] Tanzawa, T. et al. (n.d.) Introduction of a robot patient into dental education. (Report). *European Journal of Dental Education*. [Online] 16 (1), e195–e199.

[29] Hofe, R. and Moore, R.K., 2008. Towards an investigation of speech energetics using 'AnTon': an animatronic model of a human tongue and vocal tract. *Connection Science*, *20*(4), pp.319-336.

[30] Server Demirtas. (n.d.). Retrieved October 11, 2018, from www.serverdemirtas.com

[31] Ilievski, F., Chen, X., Mazzeo, A. D., Whitesides, G. M., Shepherd, R. F., Martinez, R. V., Choi, W. J., Kwok, S. W., Morin, S. A., Stokes, A., & Nie, Z. (2014). *U.S. Patent No. US 20140109560A1*. Washington, DC: U.S. Patent and Trademark Office.
[32] Mitra, A., Choudhary, S., Garg, H., H G, J. (2014). Maxillofacial prosthetic materials- an inclination towards silicones. Journal of clinical and diagnostic research : JCDR, 8(12), ZE08-13
[33] Shepherd, R. F. et al. (2011) A multi-gait soft robot. [Online] 108 (51), 20400–20403.
[34] Cao, Jiawei et al. (2017) '*Development of a soft untethered robot using artificial muscle actuators*', in [Online]. 17 April 2017 SPIE. p. 101631X–101631X–7.
[35] Onal, C.D. et al. (2017) Soft mobile robots with on-board chemical pressure generation. Springer Tracts in Advanced Robotics. [Online] 100525–540.

[36] Sun, Y., Song, Y., & Paik, J. (2013). Characterization of silicone rubber based soft pneumatic actuators (pp. 4446–4453). https://doi.org/10.1109/IROS.2013.6696995
[37] Deimel, Raphael & Brock, Oliver (2016) A novel type of compliant and underactuated robotic hand for dexterous grasping. *The International Journal of Robotics Research*. [Online] 35 (1-3), 161–185.
[38] Etheme.com. RepRap Guru DIY Prusa i3 V1 3D Printer Kit. Retrieved April 9, 2019, from https://reprapguru.com/collections/3d-printers/products/reprap-guru-diy-prusa-i3-v1-3d-printer-kit
[39] Oguntos, V. Low cost Electro-pneumatic circuit for Soft Robots. Retrieved April 21, 2019, from https://softroboticstoolkit.com/low-cost-ep-circuit
[40] Steele, Robert. (2009). Gray's Anatomy. The Anatomical Basis of Clinical Practice, 40th Edition, Susan Standring (Ed.). Churchill Livingstone Elsevier (2008), Editor-in Chief, ISBN: 978 0 8089 2371 8. The Surgeon. 7. 320. 10.1016/s1479-666x(09)80013-9.
[41] N. Docherty (2012) Netter's head and neck anatomy for dentistry, 2nd edition. *BDJ*. [Online] 212 (11), 567–568.
[42] Retrieved April 24, 2019, from http://www.uky.edu/~brmacp/oralhist/module1/lab/imgshtml/image19.htm
[43] Robinson, Sanlin S. et al. (2015) Integrated soft sensors and elastomeric actuators for tactile machines with kinesthetic sense. *Extreme Mechanics Letters*. [Online] 547–53.
[44] 1.3.0 was released! Retrieved April 28, 2019, from https://slic3r.org/
[45] Brown, Douglas. Retrieved April 28, 2019, from http://physlets.org/tracker/

XI. Appendix

Position Tracking Data

	A	B
1	Front Section Position Data	
2		
3	t	y
4	0	0.018988379
5	0.033333333	0.081926165
6	0.066666667	0.081108646
7	0.1	0.082261679
8	0.133333333	0.083220401
9	0.166666667	0.085149938
10	0.2	0.08640728
11	0.233333333	0.086405211
12	0.266666667	0.087458108
13	0.3	0.086043809
14	0.333333333	0.129367962
15	0.4	0.256381066
16	0.433333333	0.294430784
17	0.466666667	0.328102373
18	0.5	0.351260324
19	0.533333333	0.374998078
20	0.566666667	0.400991967
21	0.6	0.417864048
22	0.633333333	0.389728197
23	2.201666667	0.244847756
24	2.235	0.246155321
25	2.268333333	0.250082828
26	2.301666667	0.252938317
27	2.335	0.254323553
28	2.368333333	0.170412581

	A	B
1	Middle Section Deflection	
2		
3	t	y
4	0.6	0.151331644
5	0.633333333	0.174930509
6	0.6	0
7	0.666666667	0.123940095
8	0.7	0.132653483
9	0.733333333	0.140100463
10	0.766666667	0.150030742
11	0.8	0.160530347
12	0.833333333	0.176678723
13	0.866666667	0.19697299
14	0.9	0.270577024
15	0.933333333	0.297113203
16	0.966666667	0.308269911
17	1	0.370743733
18	1.033333333	0.36637947
19	1.066666667	0.399605167
20	1.1	0.385063056
21	1.133333333	0.388131039
22	1.166666667	0.381576442
23	1.2	0.394486149
24	1.233333333	0.396698003
25	1.266666667	0.399710145
26	1.3	0.409382108
27	1.333333333	0.416708076
28	1.366666667	0.360706189
29	1.4	0.368735897
30	1.433333333	0.377766032
31	1.466666667	0.385657459
32	1.5	0.393782932
33	1.533333333	0.416904607
34	1.566666667	0.407150798
35	1.6	0.44050552
36	1.633333333	0.45072323
37	1.666666667	0.45150251

	A	B
1	Back Section Deflection	
2		
3	t	y
4	1.5	0
5	1.6	0.12962716
6	1.633333333	0
7	1.666666667	0.168876466
8	1.7	0
9	1.735	0.180647067
10	1.768333333	0.187085089
11	1.801666667	0.190263061
12	1.835	0.195414194
13	1.868333333	0.19978724
14	1.901666667	0.203654742
15	1.935	0.20662686
16	1.968333333	0.210282952
17	2.001666667	0.212999872
18	2.035	0.217062645
19	2.068333333	0.219370577
20	2.101666667	0.222868262
21	2.135	0.226193223
22	2.168333333	0.229191386
23	2.201666667	0.232734774
24	2.235	0.234009421
25	2.268333333	0.237887508
26	2.301666667	0.240688419
27	2.335	0.242106997

Theorized Deflection Calculations

	A	B	C	D	E	F	G	H
1								
2	Middle Section							
3	**Chambers**	**Length**	**Width**	**Height**	**Force**	**I**	**E**	**Deflection**
4								
5	Air Chamber	1.44	0.1	0.15	0.65	0.000028125	18.129	71.37329
6	Air Chamber	1.24	0.1	0.15	0.65	0.000028125	18.129	39.24393
7	Passage Chamber	0.2	0.1	0.2	0.65	6.66667E-05	18.129	0.011204
8								
9							total	110.6396
10								
11	Back Section							
12								
13	Air Chamber	1.5	0.1	0.15	0.65	0.000028125	18.12971725	84.02985
14	Passage Chamber	0.2	0.1	0.2	0.65	6.66667E-05	18.12971725	0.011204
15								
16							total	168.0821
17								
18	Front Section							
19	Air Chamber	0.96	0.1	0.15	0.65	0.000028125	18.12971725	14.09787
20	Air Chamber	0.64	0.1	0.15	0.65	0.000028125	18.12971725	2.784764
21	Passage Chamber	0.2	0.1	0.2	0.65	6.66667E-05	18.12971725	0.022408
22								
23							total	16.90504